The Clp proteolytic system acts as an essential nexus for *Plasmodium* plastid biogenesis

Florentin A.[1,2], Stephens D.R.[2,3], Brooks C.F.[1,2], Baptista RP[2,4], Muralidharan V[1,2,#]

[1]Department of Cellular Biology
[2]Center for Tropical and Emerging Global Diseases
[3]Department of Pharmaceutical and Biomedical Sciences, College of Pharmacy
[4]Institute of Bioinformatics
University of Georgia, Athens, GA 30602, USA

[#]Address correspondence to: vasant@uga.edu

Abstract

The human malaria parasite, *Plasmodium falciparum,* contains a plastid called the apicoplast that functions to produce essential metabolites. Most of apicoplast proteins are encoded by the nuclear genome and it is unclear how the apicoplast controls its own proteome. Here, we investigated the prokaryotic caseinolytic-protease (Clp) system and how it regulates organelle proteostasis. Our data show that interfering with expression, activity or interactions of the Clp protease (PfClpP), chaperone (PfClpC), non-catalytic subunit (PfClpR), or substrate adaptor molecule (PfClpS) results in apicoplast loss. Using null-mutants, we demonstrated that PfClpP is essential due to its role in apicoplast biogenesis. Conditional mutants of PfClpP revealed the robustness of its proteolytic activity and its interaction with the chaperone PfClpC. Expression of a PfClpC variant with a mutation in the protease binding site demonstrated its role as an essential regulator of complex activity. A combination of several tagged Clp proteins was used for affinity purification and enabled us to determine complex composition. A CRISPR/Cas9 based system was developed and used for the expression of a catalytically-dead form of PfClpP in the background of PfClpP conditional mutants. These double-mutant parasites were used to determine the mechanisms of PfClpP oligomerization and maturation, and revealed its trans-autocatalytic properties. Further, we investigated the functions of the substrate adaptor molecule, PfClpS, and showed that it is essential for plastid biogenesis. This comprehensive study reveals the molecular mechanisms driving the function of the apicoplast PfClpP/R/C/S system and demonstrates its central role in the biogenesis of the plastid in malaria parasites.

33 # Introduction

34 The deadly malaria parasite, *Plasmodium falciparum*, has developed resistance to all currently
35 available therapies, making the discovery of new drug targets a top priority. Like most other
36 apicomplexans, the parasite contains a plastid called the apicoplast[1]. This unique organelle
37 evolved via a two-step endosymbiosis[2]; in the primary endosymbiotic event, a cyanobacterium
38 was incorporated into a eukaryotic cell to form the modern chloroplast. During the secondary
39 endosymbiotic event, a photosynthetic red alga was further taken up by a protist and led to the
40 formation of a secondary plastid[3]. Although not photosynthetic, the apicoplast harbors essential
41 prokaryotic metabolic pathways that are essential to the parasite throughout its complex life
42 cycle[4]. In a sharp contrast with its human host, the *Plasmodium* apicoplast shares molecular
43 features with prokaryotes, plants and parasites, and therefore has the potential to encompass
44 multiple parasite-specific drug targets[5,6]. Indeed, drugs that target apicoplast biology are in
45 clinical use[7,8]. Most of those drugs (e.g. Doxycycline, Clindamycin) target the prokaryotic protein
46 synthesis machinery in the apicoplast[9,10]. However, less than 10% of the apicoplast proteome is
47 encoded by its own genome. The vast majority of hundreds of apicoplast proteins are encoded
48 in the nuclear genome and are transported to the organelle via the secretory pathway[11-13]. There
49 are no data to suggest that the apicoplast controls the translation of these nuclear encoded
50 proteins, and, in fact, parasites without an apicoplast continue to express and accumulate these
51 proteins in vesicle-like structures in the cytoplasm[14,15].

52 An alternative way for the apicoplast to maintain protein homeostasis is through an organelle
53 specific proteolytic machinery. In bacteria and chloroplasts this function is executed by Clp
54 (Caseinolytic protease) proteins. This conserved family of proteins consists of ClpP proteases that
55 form multi-subunit proteolytic complexes, though their exact compositions vary widely between
56 different species and organelles[16,17]. The ClpP proteases are typically associated with Clp ATPase
57 chaperones that unfold and feed substrates into the ClpP barrel-like cavity for degradation[18,19].
58 Together, they act as key regulators that not only maintain protein homeostasis but also play
59 pivotal roles in bacterial cell division, transport, stress response and virulence[20]. In plants, Clp
60 proteins regulate the levels and activities of numerous metabolic enzymes and thus control
61 chloroplast metabolism and differentiation[21]. Some of these metabolic pathways, such as

62 isoprenoids biosynthesis, are conserved and essential in the apicoplast. Several putative Clp
63 genes have been localized to the apicoplast of *P. falciparum*. *In vitro* studies revealed some of
64 the structural features of the *Plasmodium* ClpP protease[22], the non-catalytic subunit ClpR[23] and
65 a potential substrate adaptor molecule termed ClpS[24].
66 Nevertheless, little is known about the *in vivo* function of *Plasmodium* Clps, their roles in
67 apicoplast biology or their essentiality for parasite asexual life cycle. We have previously shown
68 that the *Plasmodium* ClpC chaperone (PfClpC) is essential for parasite viability and apicoplast
69 biogenesis[15]. Here, we report the development and application of advanced molecular genetic
70 tools in a clinically important non-model organism to gain detailed mechanistic insights into
71 plastid Clp function and how this drives parasite biology. We have shown that the protease PfClpP
72 is essential and, in its absence, the entire organelle disappears. Likewise, the molecular
73 interaction between the chaperone and the protease is crucial for the complex function and
74 organelle biogenesis. A combination of several tagged Clp genes was used for affinity purification
75 and enabled us to determine complex composition and identify putative interactors, regulators
76 and substrates. A PfClpP dead-protease mutant was used for functional analysis of the proteolytic
77 activity, complex assembly and maturation. Finally, we report the biological role of PfClpS, a
78 potential Clp substrate-adaptor protein, and showed genetic and physical interactions with other
79 Clp proteins. Collectively, these data demonstrate that the Clp complex and interactions within
80 this proteolytic system acts as an essential nexus regulating apicoplast biogenesis.

Results and Discussion

PfClpP is essential for apicoplast biogenesis and survival of malaria parasites

In order to assess the biological role of the *Plasmodium* ClpP homolog, PfClpP, and test its potential as a drug target, we attempted to generate a null mutant, replacing the *pfclpp* gene with a drug marker using CRISPR/Cas9 gene editing (Figure 1A). Despite PCR evidence for successful integration into the *pfclpp* locus (Supplementary Figure 1), we repeatedly failed to retrieve live parasites following drug selection. This suggested that PfClpP is essential for parasite viability and we therefore decided to repeat the transfection in the presence of isopentenyl pyrophosphate (IPP). IPP is a small metabolite produced by the apicoplast which was shown to be the only essential function of the organelle during the asexual blood stages[14]. Transfection in the presence of IPP yielded live PfClpP knockout parasites ($PfClpP^{KO}$) on the first attempt, and integration was confirmed by PCR (Figure 1B). Using an anti-PfClpP antibody we verified that $PfClpP^{KO}$ mutants do not express PfClpP (Figure 1C). Removal of IPP from the culturing media resulted in the rapid death of the $PfClpP^{KO}$ parasites (Figure 1D). Immuno-fluorescence assays (IFA) revealed that apicoplast proteins such as Acyl Carrier Protein (ACP) and Chaperonin 60 (Cpn60) lost their typical apicoplast localization, and instead appear in vesicle-like structures (Figure 1E). Such structures are indicative of damage to organelle integrity. Indeed, quantitative Real Time PCR (qRT-PCR) showed that the entire apicoplast genome disappeared in $PfClpP^{KO}$ mutants, while the mitochondria genome was unaffected (Figure 1F). Collectively, these data demonstrate that PfClpP is essential for parasite viability, and its function is required for the biogenesis of the apicoplast organelle.

PfClpP knockdown reveals robust enzymatic activity *in vivo*

Next, we wanted to investigate the molecular mechanisms of PfClpP function. To do that, we tagged the gene with a V5 tag and the *tetR*-aptamer conditional knockdown (KD) system, enabling translational repression of PfClpP expression when anhydrotetracycline (aTc) is removed from the culturing media[25]. Using CRISPR/Cas9, we incorporated the *tetR*-aptamer regulatory cassette at the 3'end of the *pfclpp* gene, creating the $PfClpP^{apt}$ parasite line (Figure 2A). Using PCR analysis, we verified correct integration into the *pfclpp* locus (Figure 2B), and by

110 IFA we confirmed its apicoplast localization (Figure 2C). Western blot analysis revealed the
111 expected processing pattern of PfClpP; cytoplasmic fraction (I); apicoplast-localized zymogen (II)
112 and a mature protease after proteolytic removal of the pro-domain (III) (Figure 2D)[15,22]. Inducing
113 knockdown by removing aTc resulted in a significant reduction (>95%) in PfClpP protein levels,
114 however this reduction had no effect on parasite growth (Figure 2D and E). This indicated that
115 residual PfClpP protein levels were sufficient to maintain biologically functional enzymatic
116 activity without any deleterious effects. The fact that PfClpP is essential for apicoplast function,
117 and its maturation is proteolytically controlled, raised the possibility that it is post-translationally
118 regulated.
119
120 **The PfClpP and PfClpR bind each other and share common interacting partners**
121 Another putative member of the plastid Clp complex and a potential regulator of PfClpP activity
122 is PfClpR, a potential non-catalytic subunit in the Clp complex[22,23]. We therefore attempted to
123 tag PfClpR with the V5 tag and the *tetR* aptamer knockdown system (Supplementary Figure 2A).
124 Tagging *pfclpr* locus has been challenging[15] and after multiple attempts, we finally succeeded in
125 tagging the locus with the *tetR* aptamer. However, PCR analysis of the aptamer repeats region in
126 PfClpR^{apt} parasites, revealed that the number of aptamer repeats decreased during drug selection
127 from 10 to 7 (Supplementary Figure 2B). This significantly compromised knockdown efficiency
128 and prevented us from evaluating its effect on parasite replication (Supplementary Figure 2C).
129 We concluded that tagging this locus confers a fitness cost and that, like PfClpP, PfClpR may be
130 essential for plastid biogenesis. Nevertheless, the PfClpR gene was correctly tagged with the V5
131 epitope and, like PfClpP, was localized to the apicoplast (Supplementary Figure 2D). It is
132 interesting to note that the non-catalytic PfClpR comprises an inactive Clp protease domain, but
133 does not have a pro-domain, and migrates similarly on SDS-PAGE as the mature PfClpP
134 (Supplementary Figure 2E).
135 In order to identify other potential Clp interactors and regulators, we performed
136 immunoprecipitation (IP) of PfClpP^{apt} and PfClpR^{apt} parasites using the V5 tag. For large scale
137 proteomic analyses, potential Clp interactors were isolated from non-synchronized PfClpP^{apt} and
138 PfClpR^{apt} parasites using anti-V5 antibody-conjugated beads. The parental line (3D7) was used as

139 a control, and all samples were analyzed by mass spectrometry. All detected proteins were
140 filtered for predicted apicoplast localization and the abundance of each apicoplast-predicted
141 protein was calculated and averaged between biological replicates. Using individual peptide
142 abundance values, we calculated a ratio between protein abundance in IP (PfClpP or PfClpR) and
143 the parental control and set a threshold of ≥5-fold enrichment (Figure 2F and G). This resulted
144 in a list of proteins that were either detected exclusively in the Clp IP or were at least 5- fold or
145 more abundant than in the control. PfClpP IP yielded 45 proteins that are predicted to localize to
146 the apicoplast, and 29 out of these passed the threshold and were considered high-confidence
147 PfClpP interactors (Figure 2F and supplementary table 1). For PfClpR, out of 29 apicoplast-
148 predicted proteins, only 8 passed the threshold and were considered probable PfClpR interactors
149 (Figure 2G and supplementary table 1). Importantly, PfClpR appeared as a high-confidence
150 interactor for PfClpP and vice versa, suggesting a physical interaction between the two
151 components of the Clp complex. Moreover, 7 out of the 8 PfClpR positive hits were also found in
152 the PfClpP interactors list, further reinforcing them as high-confidence interactors (Figure 2H).
153 One of these seven proteins is chaperonin 60 (Cpn60), which functions in folding of proteins
154 transported to plastids[26]. The interaction of Cpn60 with the Clp complex suggests that these
155 proteins together may function as a protein quality control mechanism in the apicoplast to
156 degrade damaged and misfolded proteins.
157
158 **PfClpC interacts with mature PfClpP in the apicoplast**
159 The IP approach relied primarily on strong protein-protein interactions and could not detect
160 weaker or transient interactions with potential biological significance. For example, the mass
161 spectroscopy results did not identify PfClpC, the only apicoplast AAA+ ATPase with a conserved
162 tripeptide ClpP binding sequence[15,22]. Moreover, we have previously shown that inhibition of this
163 essential apicoplast chaperone destabilizes PfClpP[15]. In order to study factors such as PfClpC, we
164 wanted to express potential PfClpP regulators *in vivo* in PfClpP^{apt} parasites. For this purpose, we
165 developed a novel tool for stable expression in *P. falciparum*, that avoids the inconsistent
166 overexpression that occurs when using episomal plasmids. In this method, we use CRISPR/Cas9
167 editing to insert the gene of interest into a specific genomic locus, where it can be expressed

168 under an endogenous promoter. We chose the *pfhsp110c* locus, that encodes an essential
169 cytoplasmic protein that is consistently expressed throughout the parasite life cycle[27]. To test
170 whether the Hsp110 system can drive expression of apicoplast localized proteins, we introduced
171 a 2A skip peptide at the end of the gene, followed by a GFP reporter with an apicoplast transit
172 peptide (tp) derived from acyl carrier protein (ACP)[11] (tp^{ACP}-GFP, Figure 3A). Transfection and
173 integration into the into *the pfhsp110c* locus were efficient, and using IFA we confirmed robust
174 GFP expression in the apicoplast of all clones isolated (Figure 3B). Western blot analysis revealed
175 the typical double-band, consisting of a weak upper band of the cytoplasmic fraction and a more
176 prominent lower band of the apicoplast localized GFP after removal of the transit peptide (Figure
177 3C). We concluded that this method works well for expression of apicoplast proteins, and can be
178 used to study PfClpP-PfClpC interactions.
179 Using the Hsp110 expression system, we designed and expressed two isoforms of PfClpC in
180 $PfClpP^{apt}$ parasites (Figure 3A). The first was a copy of wild type PfClpC ($PfClpC^{wt}$) with a C-terminal
181 3xTy tag. We transfected $PfClpC^{wt}$, and confirmed its co-expression with PfClpP-V5 by western
182 blot (Figure 3D, left lane) and their co-localization in the apicoplast by IFA (Figure 3F, upper
183 panel). Importantly, PfClpP pulldown resulted in the co-immunoprecipitation of $PfClpC^{wt}$,
184 indicating a physical interaction between the chaperone and the protease (Figure 3E, left). The
185 reciprocal PfClpC pulldown revealed that the chaperone interacts with the mature protease (III)
186 but not with the zymogen form (II) or the full length PfClpP with the transit peptide (I) (Figure 3E,
187 right). This indicates that PfClpC and PfClpP interact only upon co-localization in the apicoplast
188 and after the proteolytic maturation of the protease.
189
190 **The Clp chaperone-protease interaction is essential for plastid biogenesis**
191 The second PfClpC variant that we expressed via the Hsp110 system had a single point mutation
192 in the 3rd amino acid of the Leu-Gly-Phe motif (aa 1101-1103) that is required for binding PfClpP
193 (F1103W, Figure 3A). The same mutation in a bacterial Clp chaperone abolished the binding to
194 the bacterial ClpP protease without affecting its folding or other chaperone activities[19]. Aside
195 from that mutation, this construct, termed $PfClpC^{F1103W}$, was identical to the first ($PfClpC^{wt}$) and
196 was similarly tagged with 3xTy and expressed from the *pfhsp110c* locus in $PfClpP^{apt}$ parasites,

197 without interfering with the endogenous *pfclpc* gene (Figure 3A). Nevertheless, multiple
198 attempts to express the PfClpC^{F1103W} variant failed, suggesting that the mutated allele has a
199 dominant negative effect on parasite viability. To rule out a general cytotoxic effect of
200 transfection or any putative lethal consequences of interfering with PfHsp110c expression, we
201 repeated transections in the presence of IPP. Since IPP is the only plastid-synthesized metabolite
202 that is essential for blood stage growth, adding IPP should enable us to express PfClpC^{F1103W} only
203 if the observed toxicity was due to specific apicoplast damage. Transfection of PfClpC^{F1103W} in the
204 presence of IPP has enabled us to retrieve live parasites. Western blot analysis revealed that in
205 these parasites, all processing of PfClpP was abolished and the only observed band was the full-
206 length cytoplasmic fraction (Figure 3D, right lane). Using microscopy, we observed that both
207 PfClpP^{apt} and PfClpC^{F1103W} did not appear in their typical apicoplast localization, and instead form
208 vesicle-like structures indicative of apicoplast damage (Figure 3F, lower panel). Clones were
209 isolated but their growth was entirely dependent on IPP, and removing it led to parasites death
210 (Figure 3G). Subsequently, quantitative real time PCR analysis revealed that the apicoplast
211 genome disappeared from PfClpC^{F1103W} parasites (Figure 3H). These results indicate that
212 interfering with the interaction between the PfClpC chaperone and the PfClpP protease inhibits
213 complex function. Further, these data suggest that the essentiality of PfClpC[15] is linked to its
214 function with PfClpP. Plant chloroplasts express several copies of ClpC chaperones, which have
215 been suggested to dynamically bind and feed different ClpP substrates into the ClpP protease[28].
216 Our data suggest that PfClpC dynamically interacts with PfClpP and this essential interaction may
217 be required for degradation of substrates to ensure apicoplast biogenesis. To our knowledge, this
218 is the first time that this interaction has been shown to be required for any plastid biogenesis.
219

220 **PfClpP oligomerizes as a zymogen and matures via trans-autoprocessing**

221 The *Plasmodium* ClpP differs structurally from its bacterial orthologues primarily because it
222 contains a transit peptide and a pro-domain (Figure 2D), both of which are removed at
223 subsequent maturations steps. Like other proteins that are transported to the plastid, PfClpP
224 possesses a transit peptide that is cleaved by a putative stromal peptide peptidase in the
225 apicoplast[12]. A second cleavage event is required for the removal of the pro-domain through an

226 unknown mechanism. It is possible that another protease is responsible for PfClpP pro-domain
227 cleavage or that this is an autocatalytic event. It also is unclear how these processing events
228 influence complex assembly and maturation of the protease. To address all of these questions
229 and to understand the mechanism of PfClpP oligomerization, we specifically interfered with the
230 proteolytic activity of PfClpP *in vivo*.
231 For this purpose, we designed a PfClpP dead-protease mutant (termed PfClpP^{DEAD}) based on
232 bacterial ClpP mutants[29]. The PfClpP^{DEAD} variant had a point mutation in the protease active site
233 (Ser264Ala) that renders it catalytically inactive (Figure 4A). It also includes the swapping of two
234 residues (Glu308Arg/ Arg285Glu) of an ion pair at the interface of the ClpP subunits[30]. The
235 purpose of this switch is to reduce the affinity between PfClpP^{DEAD} and the endogenous PfClpP in
236 order to minimize a potential dominant negative effect which may prevent us from studying
237 PfClpP maturation and oligomerization. We used the Hsp110 expression system to express this
238 Ty-tagged PfClpP^{DEAD} mutant in PfClpP^{apt} parasites (Figure 4A). The PfClpP^{DEAD} mutant co-localized
239 in the apicoplast with PfClpP^{apt} (Figure 4B). Western blot analysis showed that the PfClpP^{DEAD} is
240 processed similarly to the wild type PfClpP^{apt} to produce the cytoplasmic fraction (I); apicoplast-
241 localized zymogen (II) and active protease without the pro-domain (III) (Figure 4C). However, a
242 close examination revealed that the proteolytic maturation of the endogenous PfClpP^{apt} was
243 reduced in the presence of the PfClpP^{DEAD} variant. In the parental PfClpP^{apt} parasite line, the
244 majority of the apicoplast localized PfClpP zymogen was cleaved (fraction III, see 'parental' in
245 Figure 4C). In contrast, the processing of the same endogenous V5 tagged PfClpP was inhibited
246 in the PfClpP^{DEAD} parasites (Figure 4C). Quantification of the ratio between the processed (III) and
247 the zymogen (II) fractions, revealed a decrease of about 70% in the proteolytic processing of
248 PfClpP^{apt} (Figure 4D).
249 The shift in the processing rate could be explained by competitive binding between the two
250 PfClpP alleles. To test this model, we co-immunoprecipitated the endogenous PfClpP^{apt} (V5 tag)
251 and the PfClpP^{DEAD} (Ty tag). These experiments revealed that the two PfClpP alleles bind each
252 other, indicating that they hetero-oligomerize into a mixed complex (Figure 4E). This was
253 unexpected due to the swapping of the two residues (Glu308Arg/ Arg285Glu) of the ion pair at
254 the interface of the ClpP subunits. Unlike *B. subtilis*, where the resulting cross mutant did not

255 form heterooligomers with the wild type ClpP[30], the orthologous in PfClpP mutations potentially
256 weakened, but did not abolish cross-binding. This cross-binding revealed several molecular
257 features of PfClpP activation; the ability of each protease variant to co-immunoprecipitate not
258 only the mature form (III) but also the zymogen (II) suggests that complex assembly precedes the
259 final processing step of removing the pro-domain (Figure 4E and 4H).
260
261 **PfClpP protease activity is essential for complex function**
262 The implication of the interaction between the wild-type and dead protease mutant became
263 apparent during PfClpP^{apt} knockdown; reducing the levels of the endogenous active protease did
264 not affect PfClpP^{DEAD} expression levels but it drastically inhibited its processing (Figure 4F). The
265 inability of the parasites to remove the pro-domain from the dead protease in the absence of an
266 active PfClpP, suggests that *in vivo* the PfClpP zymogen matures through trans-autoprocessing
267 (Figure 4H). These data further suggest that the PfClpP zymogen (II) is inactive and this trans-
268 autoprocessing is essential for PfClpP activation. These data support the model that PfClpP
269 zymogen forms oligomers and this may be required for trans-autoprocessing. Further, since the
270 pro-domain in the zymogen plays a role in oligomerization of PfClpP, swapping the ion pair
271 (Glu308Arg/ Arg285Glu) on the ClpP oligomer failed to prevent hetero-oligomerization of PfClpP
272 but prevents it in bacterial ClpP. These data suggest the mechanism of maturation and
273 oligomerization for plastid Clp proteases differs from their bacterial counterparts.
274 Importantly, the robust activity of PfClpP enabled the PfClpP^{DEAD} parasites to grow normally
275 despite the presence of the mixed complexes. However, the presence of the PfClpP^{DEAD} mutant
276 rendered them more sensitive to perturbations in PfClpP levels, and under these settings,
277 knockdown of endogenous PfClpP^{apt} via removal of aTc resulted in parasite death (Figure 4G).
278 Thus, the expression of PfClpP^{DEAD} under normal PfClpP levels revealed the mechanisms of PfClpP
279 oligomerization and maturation (Figure 4H). Upon PfClpP knockdown, the lethal effects of the
280 dead-protease proved that it is the capacity to degrade substrates that is required for organelle
281 biogenesis and parasite survival (Figure 4H).
282
283 **The adaptor protein PfClpS is essential for plastid biogenesis and parasite survival**

284 Our data show that the proteolytic activity of the apicoplast Clp complex is central to its essential
285 role in regulating plastid biogenesis. Therefore, it is essential to understand the mechanisms by
286 which the apicoplast ClpP/R/C complex recognizes its substrates. In cyanobacteria and
287 chloroplasts, an adaptor protein termed ClpS, plays a vital role in selecting substrates destined
288 for degradation, and delivers them to the Clp complex[31-33]. Bioinformatic analysis has identified
289 a putative ClpS ortholog in *P. falciparum*, but its localization and physiological functions have not
290 yet been determined[24].
291 Therefore, we tagged PfClpS with a V5 tag and the *tetR*-aptamer knockdown system to generate
292 PfClpS^{apt} parasites, and confirmed integration by PCR (Figure 5A). We observed co-localization of
293 PfClpS and the apicoplast marker ACP (Figure 5C). Removal of aTc from PfClpS^{apt} parasites led to
294 a significant protein knockdown (Figure 5B). As a consequence, aTc removal inhibited parasites
295 growth, demonstrating that PfClpS is essential for parasite asexual replication (Figure 5D).
296 Importantly, this growth inhibition was completely rescued by addition of IPP, linking the
297 essential function of PfClpS to the apicoplast (Figure 5D). Microscopy revealed that apicoplast
298 proteins such as ACP accumulated in vesicle-like structures, and quantitative Real Time PCR
299 confirmed that the apicoplast genome disappears upon PfClpS knockdown (Figure 5C and E).
300 Collectively, these data show that PfClpS activity is essential for parasite viability and, similar to
301 other Clp proteins, it is required for apicoplast biogenesis.
302
303 **PfClpS associates with the Clp complex and putative substrates**
304 To examine the functional interaction between PfClpS and the Clp complex, we used the PfClpS^{apt}
305 parasites to pull down potential interactors. The immunoprecipitation and proteomics analysis
306 were performed as described earlier for PfClpP and PfClpR. Out of 39 identified potential PfClpS
307 interactors, 20 hits passed the high-confidence threshold, including PfClpR (Figure 5F and
308 Supplementary Table 1). Due to the predicted function of PfClpS, this list may be enriched with
309 putative Clp substrates. The PfClpS phenotypic data suggest that the substrates selected for
310 degradation by PfClpS are essential for apicoplast biogenesis. Including the 20 PfClpS binding
311 proteins to the PfClpP and PfClpR interactors that were identified earlier, resulted in a list of 35
312 potential Clp interactors (Supplementary table 1). Interestingly, we found a high degree of

313 overlap between hits, with roughly 50% of them shared between at least 2 different IPs
314 (PfClpP/R/S) (Figure 5G). Of a specific interest, was a small group of 5 high-confidence hits that
315 were common between all 3 IPs (Figure 5G, Supplementary table 1). These predicted apicoplast
316 proteins include a thioredoxin peroxidase, a putative RNA methyltransferase and a putative acyl
317 transferase (Figure 2H and Supplementary table 1). Interestingly, similar ClpS affinity screens in
318 *Arabidopsis* have identified substrates involved with central plastid metabolic functions[33].
319 Similarly, the parasites Clp interactors are potentially involved in very distinct metabolic
320 pathways (protein folding, RNA metabolism and lipid biosynthesis), thus emphasizing the role of
321 the *Plasmodium* Clp complex as a master regulator of apicoplast biology.
322
323 **A model for proteostasis regulation by the apicoplast Clp complex**
324 To conclude, we propose a model in which the apicoplast organelle maintains a stable proteome
325 via protein degradation. This central function is required, among other things, for organelle
326 biogenesis, and is executed and regulated by the proteolytic Clp complex (Figure 6A). As a
327 consequence, interfering with the function of different subunits of the complex leads to organelle
328 loss and parasite death. In the core of the Clp complex is PfClpP, a conserved potent serine
329 protease (Figure 6B). PfClpP is transported to the apicoplast as a zymogen, which hetero-
330 oligomerizes into a complex, and then matures into the active protease through trans-
331 autocatalytic processing. PfClpR is a non-catalytic subunit that physically interacts with other
332 complex subunits and may play a regulatory role. PfClpC is the chaperone that unfolds proteins
333 and feed them into the proteolytic core. It interacts with the mature PfClpP but not with the
334 zymogen, suggesting that it binds at a later step during complex assembly. Nevertheless, this
335 interaction is crucial for complex activity. This is supported by our previous observation that, as
336 in some bacterial Clp systems[34], PfClpC also functions as a stabilizer of the active PfClpP
337 complex[15]. Finally, a small adaptor molecule, PfClpS, binds specific substrates and deliver them
338 to the complex.
339 Targeting protein synthesis in the apicoplast is clinically effective, as manifested by the clinical
340 use of antibiotics such as doxycycline as antimalarials. However, such drugs directly affect only a
341 very small fraction of apicoplast proteins, as the majority of them are transcribed by the cell

342 nucleus and translated by the eukaryotic ribosomes in the parasite cytoplasm. Thus, a broader
343 and potentially more efficient way to disrupt the apicoplast proteome would be to target its
344 prokaryotic Clp degradation system. Indeed, due to their central function in prokaryotes, the
345 bacterial ClpP homologs lie in the center of various drug discovery programs that identified
346 potent inhibitors[35-39]. Ongoing work testing the effectiveness and specificity of these bacterial
347 inhibitors against PfClpP may lead to the identification of antimalarials[15]. Our data and model
348 suggest that small molecules inhibiting PfClpP activity will have a dual effect of reducing substrate
349 cleavage as well as preventing the further production of the mature and active PfClpP. Future
350 work is required to identify such potent inhibitors because our data show, similar to its bacterial
351 orthologs, the *Plasmodium* Clp complex is an excellent drug target.

352 ## Materials &Methods

353 **Plasmids construction**

354 Genomic DNA was isolated from *P. falciparum* using the QIAamp DNA blood kit (QIAGEN). All
355 constructs utilized in this study were confirmed by sequencing. PCR products were inserted into
356 the respective plasmids using Sequence and Ligation Independent Cloning (SLIC). Briefly, insert
357 and cut vector were mixed with a T4 DNA polymerase and incubated for 2.5 minutes at room
358 temperature, followed by 10 minutes incubation on ice and then transformed into bacteria. All
359 restriction enzymes used for this study were purchased from New England Biolabs. All
360 oligonucleotides used in this study are in Supplemental Table 2.

361 For the generation of PfClpP^{KO} donor plasmid, 500 bp from the 5'UTR of *pfclpp* (PF3D7_0307400)
362 were amplified using primers 1+2 and 500 bp from the 3'UTR of *pfclpp* were amplified using
363 primers 3+4. The human dihydrofolate reductase (hDHFR) drug selection cassette was amplified
364 from pL6 vector using primers 5+6. All three pcr products were inserted into a TOPO cloning
365 vector (ThermoFisher). Primer 7 was used in combination with primer 6 or 4 to test for accurate
366 integration in the parasite following transfections. To increase efficiency of CRISPR/Cas9
367 mediated-integration, two guide RNAs were used, targeting both ends of the PfClpP gene. For
368 expression of a C-term PfClpP guide RNA, oligos 8+9 were inserted into pUF1-Cas9-guide, and for
369 expression of the N-term PfClpP guide RNA, oligos 10+11 were independently inserted into pUF1-
370 Cas9-guide as previously described[15,40].

371 For the generation of the PfClpP^{apt} conditional mutant, 500 bps from the 3'UTR and from the C-
372 term of *pfclpp* gene were amplified pClpP-glmS vector[15] using primers 18+19 and 20+21,
373 respectively. The two products were conjugated together using PCR-sewing and inserted as one
374 piece into pMG74-tetR-Dozi vector[25]. For expression of a C-term ClpP guide RNA, oligos 8+9 were
375 inserted into pUF1-Cas9-guide.

376 For the generation of the PfClpR^{apt} conditional mutant, 500 bps from the 3'UTR and from the C-
377 term of *pfclpr* gene (PF3D7_1436800) were amplified from pClpR-glmS vector[15] using primers
378 33+34 and 35+21, respectively. The two products were conjugated together using PCR-sewing
379 and inserted as one piece into pMG74-tetR-Dozi vector[25]. Primer 36 was used in combination
380 with primer 34 or 38 to test for accurate integration in the parasite following transfections.

381 Evaluating aptamer repeats numbers was done using primers 37+38. For expression of a C-term
382 PfClpR guide RNA, oligos 39+40 were inserted into pUF1-Cas9-guide.
383 For the generation of the PfClpS^{apt} conditional mutant, 500 bps from the 3'UTR and from the C-
384 term of *pfclps* gene (PF3D7_1320100) were amplified from gDNA using primers 41+42 and 43+44,
385 respectively. The two products were conjugated together using PCR-sewing and inserted as one
386 piece into pMG74-tetR-Dozi vector[25]. Primer 45 was used in combination with primer 42 or 38 to
387 test for accurate integration in the parasite following transfections. For expression of a C-term
388 PfClpS guide RNA, oligos 46+47 were inserted into pUF1-Cas9-guide. Primers 24+25 and 25+26
389 were used to test for accurate integration in the parasite following transfections.
390 For the generation of the Hsp110 expression system, we designed a repair plasmid that contains
391 homology sequences from the *pfhsp110c* gene (PF3D7_0708800). The repair sequences include
392 the last 429 bp from *pfhsp110c* gene, followed by a 2A skip peptide, a modular tagging cassette
393 with a multiple cloning site, and the first 400 bps from *pfhsp110c* 3'UTR. The entire cassette was
394 created using gene synthesis (GeneScript) and was cloned into a puc57 backbone to create the
395 puc57-Hsp110 vector. For expression of a PfHsp110c guide RNA, oligos 22+23 were inserted into
396 pUF1-Cas9-guide.
397 For the generation of tp^{ACP}-GFP parasites, tp^{ACP}-GFP was amplified from pCEN-tp^{ACP}-GFP using
398 primers 27+28, and was inserted into puc57-Hsp110 vector (cut with MfeI and SpeI) using SLIC.
399 For the generation of PfClpC^{wt} parasites, PfClpC (PF3D7_1406600) was amplified from gDNA using
400 primers 29+32. To introduce the point mutation required for the generation of PfClpC^{F1103W}
401 parasites, PfClpC was amplified from gDNA in two pieces, using primers 29+30 and 31+32. The
402 two pieces were PCR-sewed together and inserted into puc57-Hsp110 vector (cut with MfeI and
403 NheI) using SLIC.
404 For the generation of PfClpP^{DEAD} parasites, we introduced the following point mutations into the
405 Open Reading Frame of PfClpP: Ser264Ala, Glu308Arg and Arg285Glu. The gene was synthesized
406 (GeneScrpit) and was inserted into puc57-Hsp110 vector (cut with MfeI and NheI) using SLIC.
407 **Cell culture and transfections**
408 Parasites were cultured in RPMI medium supplemented with Albumax I (Gibco) and transfected
409 as described earlier[15,41,42].

410 To generate PfClpP^{KO} parasites, a mix of three plasmids was transfected into 3D7 parasites in the
411 presence or absence of 200uM Isopentynyl Pyrophosphate (IPP, Isoprenoids LC). The plasmid mix
412 contained the PfClpP^{KO} donor plasmid and the two pUF1-Cas9-PfClpP-guide (N-terminal and C-
413 terminal guides). Drug pressure was applied 48 hours post transfection using 2.5 nM WR99210
414 (Sigma) to select for parasites expressing hDHFR.
415 To generate PfClpP^{apt}, PfClpR^{apt} and PfClpS^{apt} parasites, a mix of two plasmids was transfected
416 into 3D7 parasites in the presence of 0.5 uM anhydrotetracycline (aTc, Cayman Chemicals). The
417 plasmid mix contained 50 ug of pUF1-Cas9-guide (expressing the relevant guide: PfClpP/R/S) and
418 50 ug of the pMG74 based donor plasmid (with the related homology regions). Drug pressure
419 was applied 48 hours post transfection using 2.5 ug/ml Blasticidin (BSD, Sigma). For each
420 transfection, at least 2 clones were isolated via limiting dilution and used for subsequent
421 experiments.
422 To generate tp^{ACP}-GFP, PfClpP^{DEAD}, PfClpC^{wt} and PfClpC^{F1103W} parasites, a mix of two plasmids was
423 transfected into PfClpP^{apt} parasites. For each different transfection the primers mix contained 2
424 plasmids; 50 ug of pUF1-Cas9-PfHsp110c-guide and 50 ug of the relevant marker-less puc57-
425 Hsp110 repair plasmid (puc57-Hsp110-tp^{ACP}-GFP/ puc57-Hsp110-PfClpP^{DEAD}/ puc57-Hsp110-
426 PfClpC^{wt}/ puc57-Hsp110-PfClpC^{F1103W}, respectively). For PfClpC^{F1103W}, transfections were
427 performed in the presence or absence of 200μM IPP (Isoprenoids LC). Drug pressure was applied
428 48 hours post transfection, using 1 μM DSM1 (BEI Resources), selecting only for Cas9 expression.
429 DSM1 was removed from the culturing media once parasites clones were isolated using limiting
430 dilution.
431 **Growth assays**
432 For PfClpP^{apt}, PfClpP^{DEAD}, PfClpR^{apt} and PfClpS^{apt}, asynchronous parasite cultures were washed 5
433 times and incubated without aTc. For PfClpP^{KO} and PfClpC^{F1103W}, parasite cultures were washed
434 once and incubated without IPP. Throughout the course of the experiment parasites were sub-
435 cultured to maintain the parasitemia between 1-5% and parasitemia was monitored every 24
436 hours via flow cytometry. Relative parasitemia at each time point was back calculated based on
437 actual parasitemia multiplied by the relevant dilution factors. Parasitemia in the presence of aTc

438 or IPP at the end of each experiment was set as the highest relative parasitemia and was used to
439 normalize parasites growth. Data were analyzed using Prism (GraphPad Software, Inc.)
440 For IPP rescue (PfClpS^{apt}, PfClpP^{KO} and PfClpC^{F1103W}) media was supplemented with 200 μM of IPP
441 (Isoprenoids LC) in PBS.
442

443 **Western blot**

444 Western blots were performed as described previously[43]. Briefly, parasites were collected and
445 host red blood cells were permeabilized selectively by treatment with ice-cold 0.04% saponin in
446 PBS for 10 min, followed by a wash in ice-cold PBS. Cells were lysed using RIPA buffer, sonicated,
447 and cleared by centrifugation at 4°C. The antibodies used in this study were mouse anti GFP, JL8
448 (Roche, 1:3000), mouse anti Ty1 SAB4800032 (Sigma, 1:1000), rabbit anti-V5, D3H8Q (Cell
449 Signaling, 1:1000), mouse anti-V5, TCM5 (eBioscience^{TM}, 1:1000), mouse monoclonal anti-PMV
450 (from D. Goldberg, 1:400), rabbit polyclonal anti-EF1α (from D. Goldberg, 1:2000) and rabbit
451 polyclonal anti-PfClpP (from W. Houry, 1:4000). The secondary antibodies that were used are
452 IRDye 680CW goat anti-rabbit IgG and IRDye 800CW goat anti-mouse IgG (LICOR Biosciences,
453 1:20,000). The Western blot images and quantifications were processed and analyzed using the
454 Odyssey infrared imaging system software (LICOR Biosciences).

455 **Microscopy and image processing**

456 For IFA cells were fixed using a mix of 4% Paraformaldehyde and 0.015% glutaraldehyde and
457 permeabilized using 0.1% Triton-X100. Primary antibodies used are mouse anti Ty1 SAB4800032
458 (Sigma, 1:500), rabbit anti-V5, D3H8Q (Cell Signaling, 1:100), mouse anti-V5, TCM5
459 (eBioscience^{TM}, 1:100), rabbit anti-Cpn60 (from B. Striepen, 1:1,000) and rabbit anti-ACP (from
460 G. Mcfadden, 1:5,000). Secondary antibodies used are Alexa Fluor 488 and Alexa Fluor 546 (Life
461 Technologies, 1:100). Cells were mounted on ProLong Diamond with DAPI (Invitrogen). For live
462 cell imaging of tp^{ACP}-GFP parasites were incubated with 8 μM Hoechst (ThermoFisher Scientific)
463 in PBS. The imaging was performed using DeltaVision II microscope system with an Olympus IX-
464 71 inverted microscope using a 100X objective. All images were collected as Z-stack, were
465 deconvolved using the DVII acquisition software SoftWorx and displayed as maximum intensity
466 projection. Image processing, analysis and display were preformed using SoftWorx and Adobe

467 Photoshop. Adjustments to brightness and contrast were made for display purposes.

468 **Flow cytometry**

469 Aliquots of parasite cultures (5μl) were stained with 8 μM Hoechst (ThermoFisher Scientific) in
470 PBS. The fluorescence profiles of infected erythrocytes were measured by flow cytometry on a
471 CytoFlex S (Beckman Coulter, Hialeah, Florida) and analyzed by FlowJo software (Treestar, Inc.,
472 Ashland, Oregon). The parasitemia data were fit to standard growth curve using Prism (GraphPad
473 Software, Inc.).

474 **Quantitative Real Time PCR**

475 Asynchronous parasites (PfClpP^{KO} and PfClpC^{F1103W}) or Synchronized ring stage parasites
476 (PfClpS^{apt}) samples were collected and genomic DNA was purified using QIAamp blood kits
477 (Qiagen). Primers that amplify segments from genes encoded by nuclear or organelles genomes
478 were designed using RealTime qPCR Assay Entry (IDT). The following primer sequences were
479 used: *cht1* (nuclear)- 12+13; *tufA* (apicoplast)- 14+15; *cytb3* (mitochondria)- 16+17. Reactions
480 contained template DNA, 0.5 uM of gene specific primers, and IQ^{TM} SYBR Green Supermix
481 (BIORAD). Quantitative real-time PCR was carried out in triplicates and was performed at a 2-step
482 reaction with 95°C denaturation and 56°C annealing and extension for 35 cycles on a CFX96 Real-
483 Time System (BIORAD). Relative quantification of target genes was determined using Bio-Rad CFX
484 manager 3.1 software. Standard curves for each primers set were obtained by using different
485 dilutions of control gDNA as template, and were used to determine primers efficiency. The
486 organelle: nuclear genome ratio of mutant parasites was calculated relative to that of the control.
487 Unpaired t-test (Benjamini, Krieger, Yekutieli) was used to calculate significance between control
488 and mutants.

489

490 **Immunoprecipitation**

491 For the pull-down proteomic analysis of PfClpP^{apt}, PfClpR^{apt} and PfClpS^{apt} parasites, the parental
492 line (wild type clone 3D7) was used a control and all pulldown experiments were done in
493 duplicates using two different clones. Immunoprecipitation protocols were performed using anti-
494 V5 antibody as previously described[44]. Briefly, pellets from 10^9 parasites were isolated using cold

495 saponin and were lysed and sonicated in Extraction Buffer (40 mM Tris HCL pH 7.6, 150 mM KCL,
496 and 1 mM EDTA) supplemented with 0.5% NP-40 (VWR) and HALT protease inhibitor (Thermo).
497 10% of the sample was kept for later analysis (input sample). Rabbit anti-V5 (Cell Signaling,
498 D3H8Q) antibody was crosslinked to DynabeadsTM protein G (Invitrogen) beads using 5 mM BS3
499 crosslinker (CovaChem) and then incubated with the supernatant at 4°C. Washes were
500 performed using a magnetic rack (Life technologies). Samples were run on SDS-page and gel slices
501 were sent to mass spectrometry analysis.
502 For the co-Immunoprecipitation of PfClpP^{DEAD} and PfClpP^{apt}, 2 samples of PfClpP^{DEAD} clone C9,
503 each containing 10^8 parasites were isolated as described above. Pellets were incubated with
504 either anti-Ty antibody (SAB4800032, Sigma) or with anti-V5 antibody (Cell Signaling, D3H8Q).
505 Input and IP samples were loaded on SDS-page and blotted with anti-Ty antibody (SAB4800032,
506 Sigma) or with anti-V5 (Cell Signaling, D3H8Q).
507 For the co-Immunoprecipitation of PfClpC^{wt} and PfClpP^{apt}, 2 samples of PfClpC^{wt}, each containing
508 10^9 parasites were isolated as described above. Pellets were incubated with either anti-Ty
509 antibody (SAB4800032, Sigma) or with anti-V5 (Cell Signaling, D3H8Q) antibody. Input and IP
510 samples were loaded on SDS-page and blotted with Ty antibody (SAB4800032, Sigma) or with
511 anti-V5 (Cell Signaling, D3H8Q).
512
513 **Mass spectrometry and data analysis**
514 PfClpP^{apt}, PfClpR^{apt} and PfClpS^{apt} samples were sent to the proteomics shared resources in Fred
515 Hutchinson Cancer Research Center and were run on the OrbiDEAD Elite. The data were searched
516 using Proteome Discoverer 2.2 against the UP000001450 *Plasmodium falciparum* (Uniprot Nov
517 2018) database including common contaminants using Sequest HT and Percolator for validation.
518 The search results were filtered for high confidence, with a strict 1% false discovery rate.
519 All detected proteins were analyzed for predicted apicoplast localization using four different
520 bioinformatic algorithms: (i)PATS[45]; (ii)ApicoAP[46]; (iii)PlasmoAP[13]; and (iv) PlastNN[47]. We then
521 compared results from all four algorithms and used known apicoplast proteins (such as Clp
522 proteins) to estimate false-negative and false-positive rates for each algorithm. Based on these
523 data, we chose to filter for apicoplast prediction using PlasmoAP, since it had a lower false-

524 negative rate than PlastNN (higher sensitivity) and higher accuracy than the first two algorithms.
525 The abundance of each apicoplast-predicted protein was calculated by summing the total
526 intensities (MS1 values) of all matched peptides for each selected protein, and normalizing by
527 the total summed intensity of all matched peptides in the sample, as previously described[47]. The
528 resulted calculated value was then averaged between replicates. To filter for high confidence
529 hits, we calculated the abundance ratio between Clp IP (PfClpP/ PfClpR/ PfClpS) and the parental
530 control, and set a threshold of ≥5 fold enrichment.

531 **ACKNOWLEDGMENTS**

532 We thank Geoffrey McFadden for anti-ACP antibody, Boris Striepen for anti-CPN60 antibody,
533 Walid Houry for anti-PfClpP antibody, and Dan Goldberg for anti-PMV, and anti-EF1α antibodies;
534 Julie Nelson at the CTEGD Cytometry Shared Resource Laboratory for help with flow cytometry
535 and analysis; and Muthugapatti Kandasamy at the Biomedical Microscopy Core at the University
536 of Georgia for help with microscopy. We acknowledge assistance of the Proteomics Resource at
537 Fred Hutchinson Cancer Research Center for mass spectrometry. This work was supported the
538 American Heart Association Postdoctoral Fellowship to A. F., and the U.S. National Institutes of
539 Health (R21AI128195) to V. M.

540 **Figure 1**

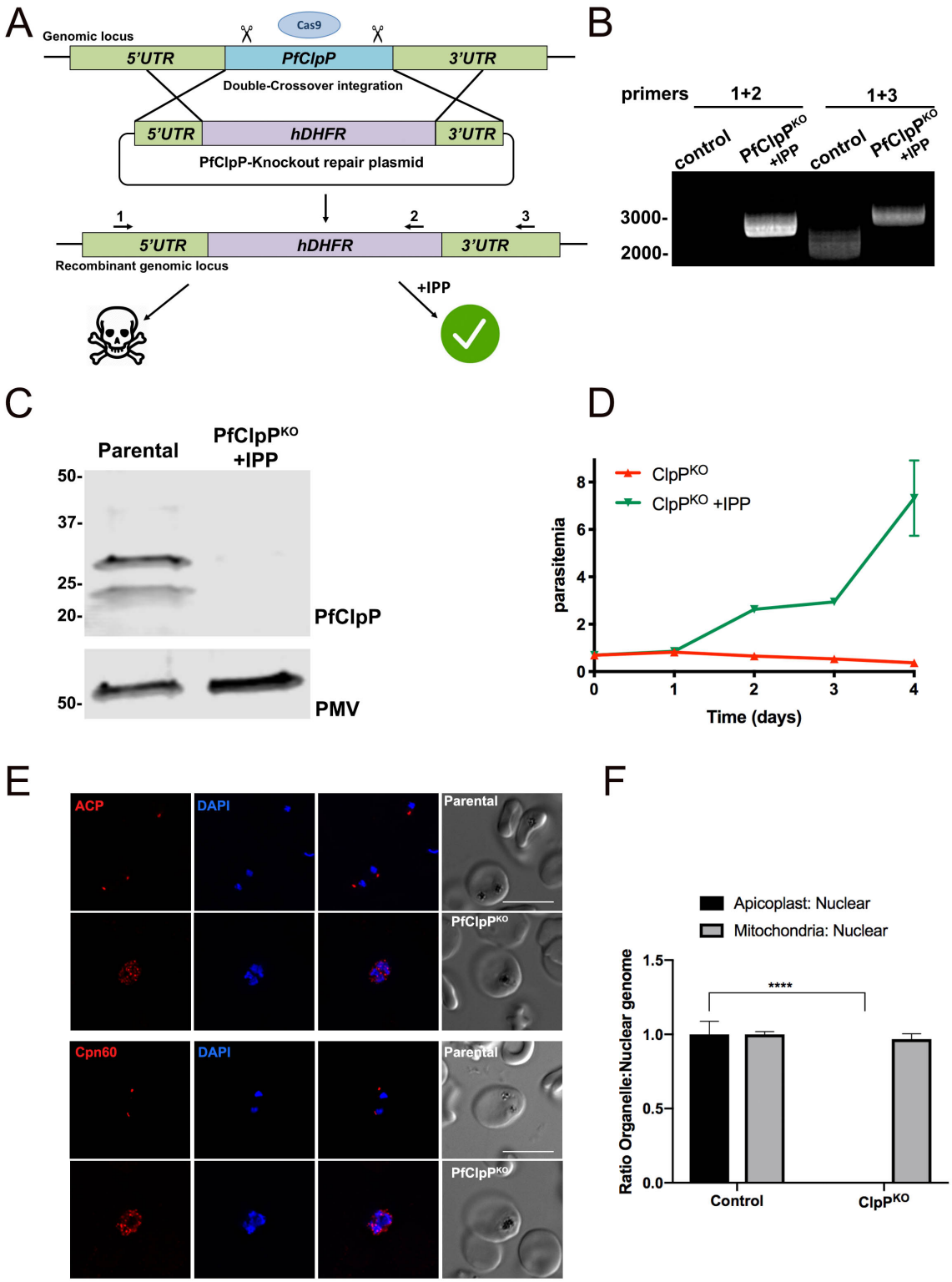

541

542 **Figure 1**

543 A. Generation of PfClpP knockout (PfClpP^{KO}) parasites. CRISPR/Cas9 and two guide RNAs (gRNA)
544 targeting the N- and the C-termini of PfClpP were used to facilitate integration. The repair
545 plasmid contained 500bps homology regions to the 5'UTR and the 3'UTR of the *pfclpp* locus
546 flanking the human dihydrofolate reductase selection marker (hDHFR). Through double
547 crossover integration and drug selection, the gene was replaced with the drug marker. This
548 strategy failed to retrieve live parasites unless IPP was added during drug selection.

549 B. PCR test confirming hDHFR integration at the *pfclpp* locus in the presence of IPP. Genomic
550 DNA was purified from transfected parasites. Primers 1+2 (see methods) were used to
551 amplify an integration specific product. Primers 1+3 were used to amplify the region between
552 the 5'UTR and 3'UTR of *pfclpp*, as illustrated in A. A shift of 1 KB corresponds to the integration
553 of the hDHFR cassette.

554 C. Western blot of parasite lysates from parental line and PfClpP^{KO} parasites probed with
555 antibodies against PfClpP and Plasmepsin V (PMV, loading control), confirming loss of PfClpP
556 expression in the null mutants. The protein marker sizes that co-migrated with the probed
557 protein are shown on the left.

558 D. IPP was removed from PfClpP^{KO} parasites and parasitemia was monitored every 24 hours over
559 4 days via flow cytometry. Data are represented as mean ± S.E.M. (n=3 technical replicates).
560 One representative experiment out of three biological replicates is shown.

561 E. Immunofluorescence imaging of fixed PfClpP^{KO} parasites stained with antibodies against ACP
562 (Acyl Carrier Protein), and DAPI (upper panel) or Cpn60 (Chaperonin 60) and DAPI (lower
563 panel). Both ACP and Cpn60 lose their typical apicoplast localization in PfClpP^{KO} and appear
564 in vesicle-like structures. Z-stack images were deconvolved and projected as a combined
565 single image. Representative images from biological replicates are shown. Scale bar, 5μm.

566 F. Genomic DNA samples were collected from PfClpP^{KO} and control parasites for quantitative
567 Real Time PCR analysis. Apicoplast: nuclear genome ratio was calculated for each sample.
568 Mitochondria: nuclear genome ratio served as a control. Genome ratios were normalized to
569 control parasites. Apicoplast genome is completely lost in PfClpP^{KO} mutants, while the
570 mitochondria genome was unaffected. One representative experiment (out of 3 biological

571 replicates) is shown. Data are represented as mean ± S.E.M (n=3 technical replicates,
572 unpaired t-test, P value =0.00013)

573 **Figure 2**

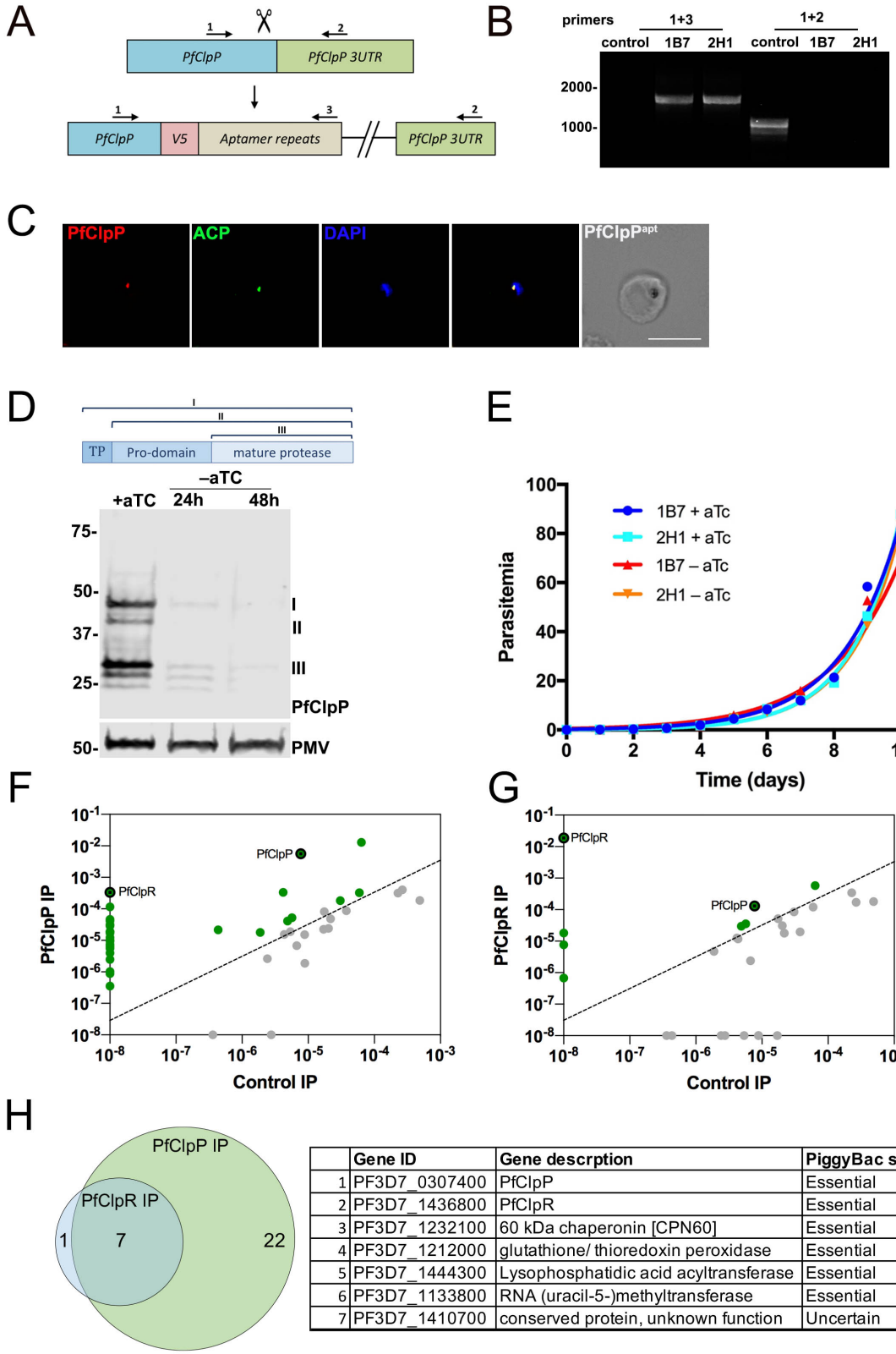

	Gene ID	Gene descrption	PiggyBac screen
1	PF3D7_0307400	PfClpP	Essential
2	PF3D7_1436800	PfClpR	Essential
3	PF3D7_1232100	60 kDa chaperonin [CPN60]	Essential
4	PF3D7_1212000	glutathione/ thioredoxin peroxidase	Essential
5	PF3D7_1444300	Lysophosphatidic acid acyltransferase	Essential
6	PF3D7_1133800	RNA (uracil-5-)methyltransferase	Essential
7	PF3D7_1410700	conserved protein, unknown function	Uncertain

574 **Figure 2**

575 A. Diagram showing integration of the *tetR*-aptamer system into the *pfclpp* locus. The Cas9
576 nuclease together with a PfClpP-specific gRNA introduces a double-stranded break at the C-
577 terminus of the *pfclpp* gene. The repair plasmid provides the template for double-crossover
578 homologous recombination, introducing a 3xV5 tag and the *tetR-Dozi* cassette, including 10
579 aptamer repeats.

580 B. PCR test confirming *tetR-Dozi* integration at the *pfclpp* locus. gDNA was purified from 2
581 independently selected mutant clones (1B7 and 2H1). Primers 1,2,3 (see methods) were used
582 to amplify the native locus (1+2) or an integration specific product (1+3), as illustrated in the
583 diagram in A.

584 C. Immunofluorescence imaging of fixed PfClpP^{apt} parasites clone 1B7 stained with antibodies
585 recognizing PfClpP (αV5, red), ACP (αAcyl Carrier Protein, green), and DAPI. Z-stack images
586 were deconvolved and projected as a combined single image. Representative images from
587 three biological replicates are shown. Scale bar, 5μm.

588 D. PfClpP^{apt} parasites were incubated without aTc for 2 days, and lysates were isolated every 24
589 hr. Western blot shows parasite lysates probed with antibodies recognizing PfClpP (αV5) and
590 Plasmepsin V (αPMV, loading control). The expected processing pattern of PfClpP is depicted:
591 cytoplasmic fraction (I); apicoplast-localized zymogen (II) and mature protease after removal
592 of the pro-domain (III). A significant reduction in PfClpP protein levels in achieved after 24
593 hours. The protein marker sizes that co-migrated with the probed protein are shown on the
594 left.

595 E. Two independent mutant clones (1B7 and 2H1) of PfClpP^{apt} parasites were grown with or
596 without 0.5 μM aTc, and parasitemia was monitored every 24 hr over 11 days via flow
597 cytometry. 100% of growth represents the highest value of calculated parasitemia (final
598 parasitemia in the presence of aTc). Data are fit to an exponential growth equation and are
599 represented as mean ± SEM (n= 3 technical replicates). One representative experiment out
600 of three biological replicates is shown.

601 F. Mass spectrometry analysis of PfClpP Immunoprecipitate, isolated from PfClpP^{apt} parasite
602 lysates using anti V5 antibody-conjugated beads. The parental line 3D7 was used a control

603 and pulldown experiments were done in duplicates using two independent PfClpP^{apt} clones;
604 1B7 and 2H1. All proteins detected in both biological replicates were filtered for predicted
605 apicoplast localization. The abundance of each apicoplast-predicted protein was calculated
606 and averaged between replicates. To filter for high confidence hits, we set a threshold of ≥5
607 folds enrichment in Clp IP vs. parental control. For PfClpP, 29 out of 45 proteins have passed
608 the threshold and were defined as high-confidence hits, including PfClpR.

609 *G.* PfClpR was immunoprecipitated from lysates of PfClpR^{apt} parasites using anti V5 antibody-
610 conjugated beads. Biological replicates were performed for both parental control and
611 PfClpR^{apt} parasites (Clones A10 and B5). The sample analysis and data were processed as in F
612 and 8 out of 29 hits passed the threshold, including PfClpP.

613 H. Venn diagram and a table showing the overlap between proteins identified in PfClpP and
614 PfClpR pulldowns. Out of the 8 PfClpR positive hits, 7 were also found in the PfClpP list,
615 outlining them as high confidence interactors.

616 **Figure 3**

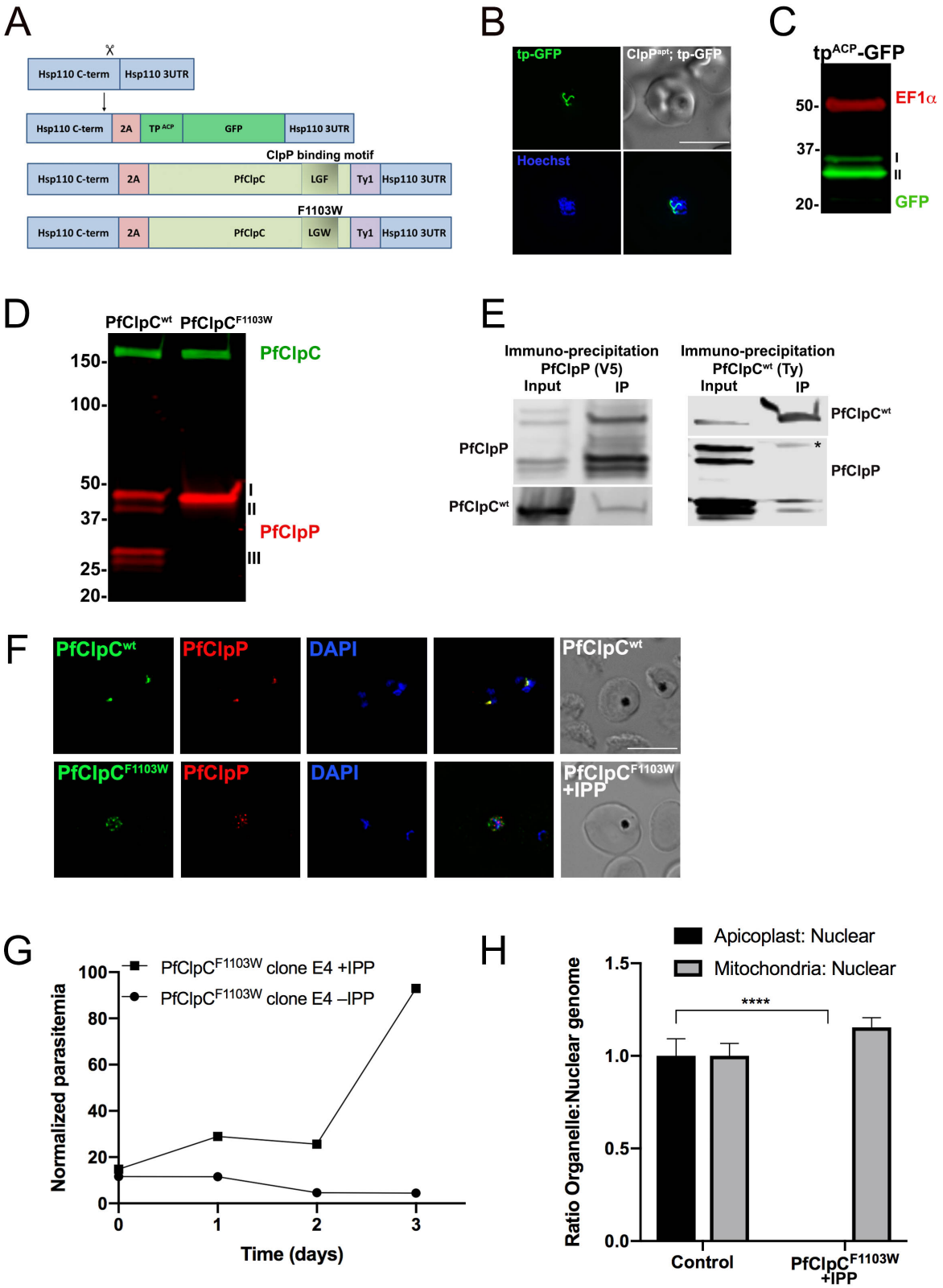
A
Hsp110 C-term
Hsp110 3UTR
2A
TP ACP
GFP
ClpP binding motif
PfClpC
LGF
Ty1
F1103W
LGW
B
tp-GFP
ClpPapt; tp-GFP
Hoechst
C
tpACP-GFP
EF1α
50-
37-
20-
I
II
GFP
D
PfClpCwt
PfClpCF1103W
PfClpC
150-
100-
50-
37-
25-
20-
PfClpP
III
E
Immuno-precipitation
PfClpP (V5)
Input
IP
PfClpCwt (Ty)
PfClpP
PfClpCwt
*
F
PfClpCwt
PfClpP
DAPI
PfClpCF1103W
PfClpCF1103W +IPP
G
PfClpCF1103W clone E4 +IPP
PfClpCF1103W clone E4 –IPP
Normalized parasitemia
Time (days)
H
Apicoplast: Nuclear
Mitochondria: Nuclear
Ratio Organelle:Nuclear genome
****
Control
PfClpCF1103W +IPP

617 **Figure 3**

618 A. Diagram showing integration and expression through the Hsp110 expression system. Cas9
619 nuclease together with a gRNA targeting the *pfhsp110c* locus, introduces a double-stranded
620 break at the c-terminus of the *pfHsp110c* gene. The repair plasmid provides two homology
621 regions for homologous recombination, flanking a 2A skip peptide and a tagged gene of
622 interest. Using this method, we introduced an apicoplast-localized GFP, a copy of wild type
623 PfClpC tagged with 3xTy (PfClpC^{wt}) and a PfClpC variant with a mutation in the putative PfClpP
624 binding site (PfClpC^{F1103W}).

625 B. Live fluorescence microscopy visualizing the apicoplast localized GFP (tp^{ACP}-GFP) expressed
626 through the *pfHsp110c* locus in PfClpP^{apt} parasites. Parasite DNA was stained with Hoechst.
627 Representative image from biological replicates is shown.

628 C. Western blot of parasite lysates from tp^{ACP}-GFP parasites probed with antibodies against GFP
629 and EF1α (loading control). The protein marker sizes that co-migrated with the probed
630 protein are shown on the left.

631 D. Western blot of parasite lysates from PfClpC^{wt} and PfClpC^{F1103W} parasites probed with
632 antibodies against V5 (PfClpP, red) and Ty (PfClpC, green). Loss of all processing of PfClpP in
633 PfClpC^{F1103W} parasites is due to apicoplast loss. The protein marker sizes that co-migrated
634 with the probed protein are shown on the left.

635 E. Co-Immunoprecipitation of PfClpP and PfClpC in PfClpP^{apt}; PfClpC^{wt} parasites. 10^9 parasites
636 were isolated and pellets were incubated with either anti-V5 antibody-conjugated beads
637 (PfClpP pulldown, left) or anti-Ty antibody-conjugated beads (PfClpC pulldown, rights). Input
638 and IP samples were loaded on SDS-page and blotted with anti-Ty (PfClpC) and anti-V5
639 (PfClpP) antibodies. An interaction between the protease and the chaperone is observed. The
640 residual heavy chain of the anti-Ty antibody that eluted with the IP sample despite the cross
641 linker is also denoted (*).

642 F. Immunofluorescence microscopy of fixed PfClpC^{wt} and PfClpC^{F1103W} parasites stained with
643 antibodies against V5 (PfClpP, red), Ty (PfClpC, green), and DAPI (DNA). The two proteins co-
644 localize in the apicoplast in PfClpC^{wt} parasites but appear in vesicle-like structures in
645 PfClpC^{F1103W} parasites. Z-stack images were deconvolved and projected as a combined single

646 image. Representative images from one of two biological replicates are shown. Scale bar,
647 5μm.
648 G. IPP was removed from PfClpC^{F1103W} parasites and parasitemia was monitored every 24 hours
649 over 3 days via flow cytometry. 100% of growth represents the highest value of calculated
650 parasitemia (final parasitemia in the presence of IPP). Data are represented as mean ± S.E.M.
651 (n=3). One representative experiment out of two biological replicates is shown.
652 G. Genomic DNA samples were collected from PfClpC^{F1103W} and control parasites for
653 quantitative Real Time PCR analysis. Apicoplast: nuclear genome ratio was calculated for each
654 sample. Mitochondria: nuclear genome ratio served as a control. Genome ratios were
655 normalized to control parasites. Data are represented as mean ± S.E.M (n=3 technical
656 replicates, unpaired t-test, P value=0.00025). One representative experiment out of two
657 biological replicates are shown.

658 **Figure 4**

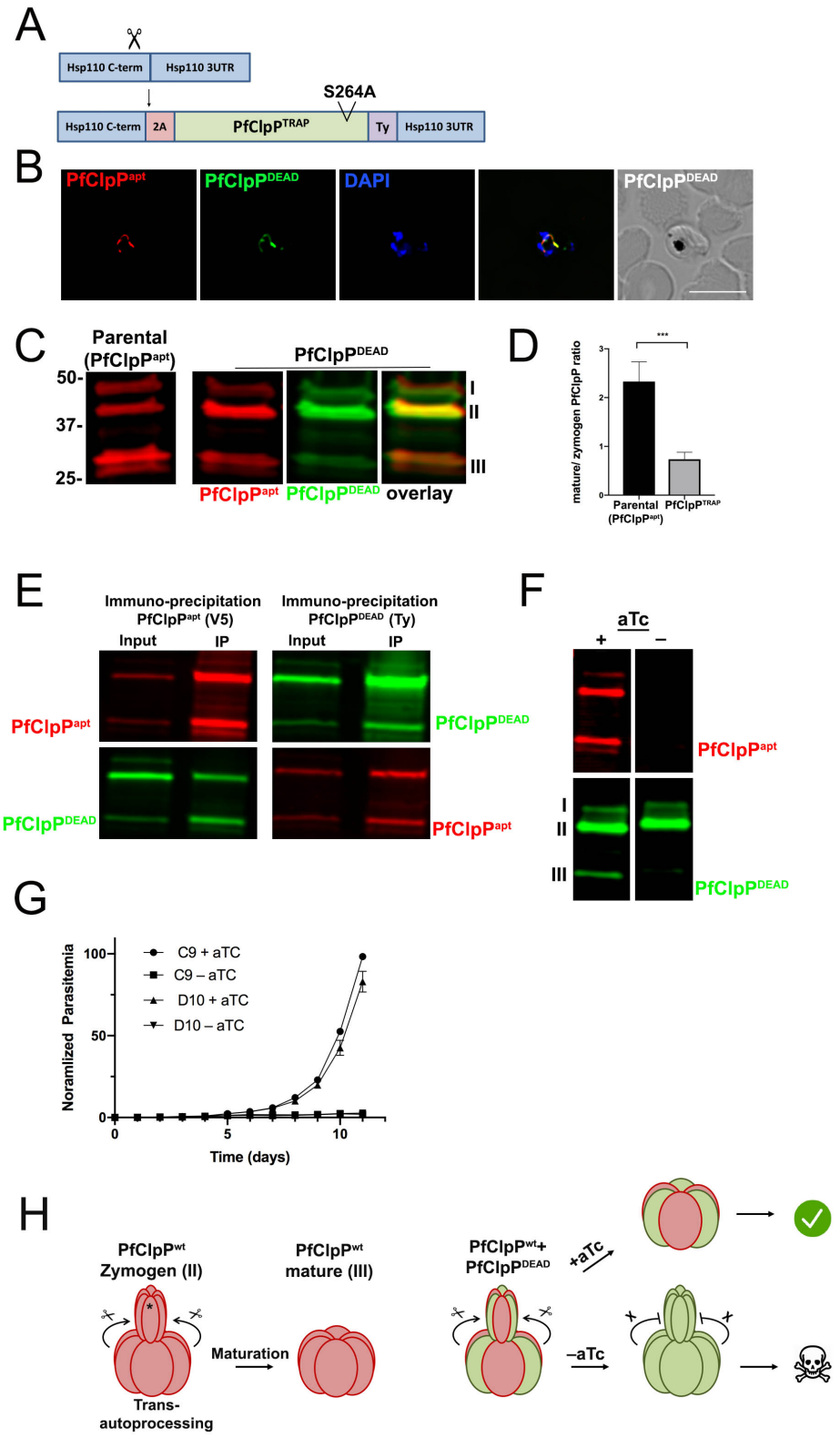
A
Hsp110 C-term
Hsp110 3UTR
S264A
Hsp110 C-term
2A
PfClpP^TRAP
Ty
Hsp110 3UTR
B
PfClpP^apt
PfClpP^DEAD
DAPI
PfClpP^DEAD
C
Parental (PfClpP^apt)
PfClpP^DEAD
50-
37-
25-
I
II
III
PfClpP^apt
PfClpP^DEAD
overlay
D
mature/ zymogen PfClpP ratio
***
Parental (PfClpP^apt)
PfClpP^TRAP
E
Immuno-precipitation PfClpP^apt (V5)
Immuno-precipitation PfClpP^DEAD (Ty)
Input
IP
Input
IP
PfClpP^apt
PfClpP^DEAD
PfClpP^DEAD
PfClpP^apt
F
aTc
+
–
PfClpP^apt
I
II
III
PfClpP^DEAD
G
Noramlized Parasitemia
C9 + aTC
C9 – aTC
D10 + aTC
D10 – aTC
Time (days)
H
PfClpP^wt Zymogen (II)
PfClpP^wt mature (III)
Maturation
Trans-autoprocessing
PfClpP^wt+ PfClpP^DEAD
+aTc
–aTc

659 **Figure 4**

660 A. Diagram showing integration and expression of 3xTy-tagged PfClpP^{DEAD} variant into the
661 *pfHsp110c* locus. Cas9 nuclease in complex with a gRNA targeting this locus introduces a
662 double-stranded break at the C-terminus of the *pfHsp110c* gene. The repair plasmid provides
663 two homology regions for homologous recombination, flanking a 2A skip peptide and the
664 3xTy-tagged PfClpP^{DEAD}. This catalytically-inactive PfClpP variant has a point mutation in the
665 protease active site (Ser264Ala).

666 B. Immunofluorescence microscopy of fixed PfClpP^{apt}; PfClpP^{DEAD} parasites stained with
667 antibodies against V5 (endogenous PfClpP^{apt}, red), Ty (PfClpP^{DEAD}, green) and DAPI (DNA). The
668 two proteins co-localize in the apicoplast. Z-stack images were deconvolved and projected as
669 a combined single image. Representative image from one of two biological replicates is
670 shown. Scale bar, 5μm.

671 C. Western blot of parental PfClpP^{apt} and PfClpP^{apt};PfClpP^{DEAD} parasite lysates probed with
672 antibodies against V5 (endogenous *wild type* PfClpP, red) and Ty (PfClpP^{DEAD}, green). The
673 identical migration pattern indicates that PfClpP^{apt} and PfClpP^{DEAD} are similarly processed. The
674 protein marker sizes that co-migrated with the probed protein are shown on the left.

675 D. The ratio between the mature and zymogen forms of endogenous PfClpP (V5-tagged) is
676 decreased upon PfClpP^{DEAD} expression, indicating that the dead variant interferes with the
677 processing of the endogenous protease. Quantification of the ratio of V5 tagged PfClpP II and
678 III fractions from 3 biological replicates (p-value =0.0007, unpaired t-test).

679 E. Co-Immunoprecipitation of PfClpP^{apt} (V5-tagged) and PfClpP^{DEAD} (Ty-tagged). 10^8 parasites
680 were isolated and pellets were incubated with either anti-V5 antibody-conjugated beads
681 (left) or anti-Ty antibody-conjugated beads (right). Input and IP samples were loaded on SDS-
682 page and blotted with anti-Ty and anti-V5 antibodies. The robust interaction between the
683 two Clp protease variants suggests that they hetero-oligomerize into a mixed complex.

684 F. PfClpP^{apt};PfClpP^{DEAD} parasites were incubated without aTc for 24 hours, and lysates were
685 isolated. Western blot of these lysates was probed with antibodies against V5 (endogenous
686 PfClpP, red) and Ty (PfClpP^{DEAD}, green). PfClpP^{apt} knockdown results in the disappearance of

687 the processed form of PfClpP^{DEAD}, suggesting that the protease maturates through trans-
688 autoprocessing.

689 G. PfClpP^{apt};PfClpP^{DEAD} parasite clones (C9 and D10) were grown with or without aTc, and
690 parasitemia was monitored every 24 hr over 11 days via flow cytometry. 100% of growth
691 represents the highest value of calculated parasitemia (final parasitemia in the presence of
692 aTc). Data are represented as mean ± SEM (n=3 technical replicates). One representative
693 experiment out of two biological replicates is shown.

694 H. A model illustrating the mechanisms of PfClpP oligomerization and maturation. PfClpP
695 oligomerizes as a zymogen and subsequently matures by removing its pro-domain (denoted
696 with *) via trans-autoprocessing. In the presence of the PfClpP^{DEAD} variant, a mixed complex
697 is assembled and due to the robustness of PfClpP proteolytic activity, there is no effect on
698 parasite growth. Upon aTc removal expression levels of endogenous PfClpP are dramatically
699 reduced, and predominantly PfClpP^{DEAD} zymogen complexes are formed. Consequently,
700 substrate degradation is inhibited and the parasites die.

Figure 5

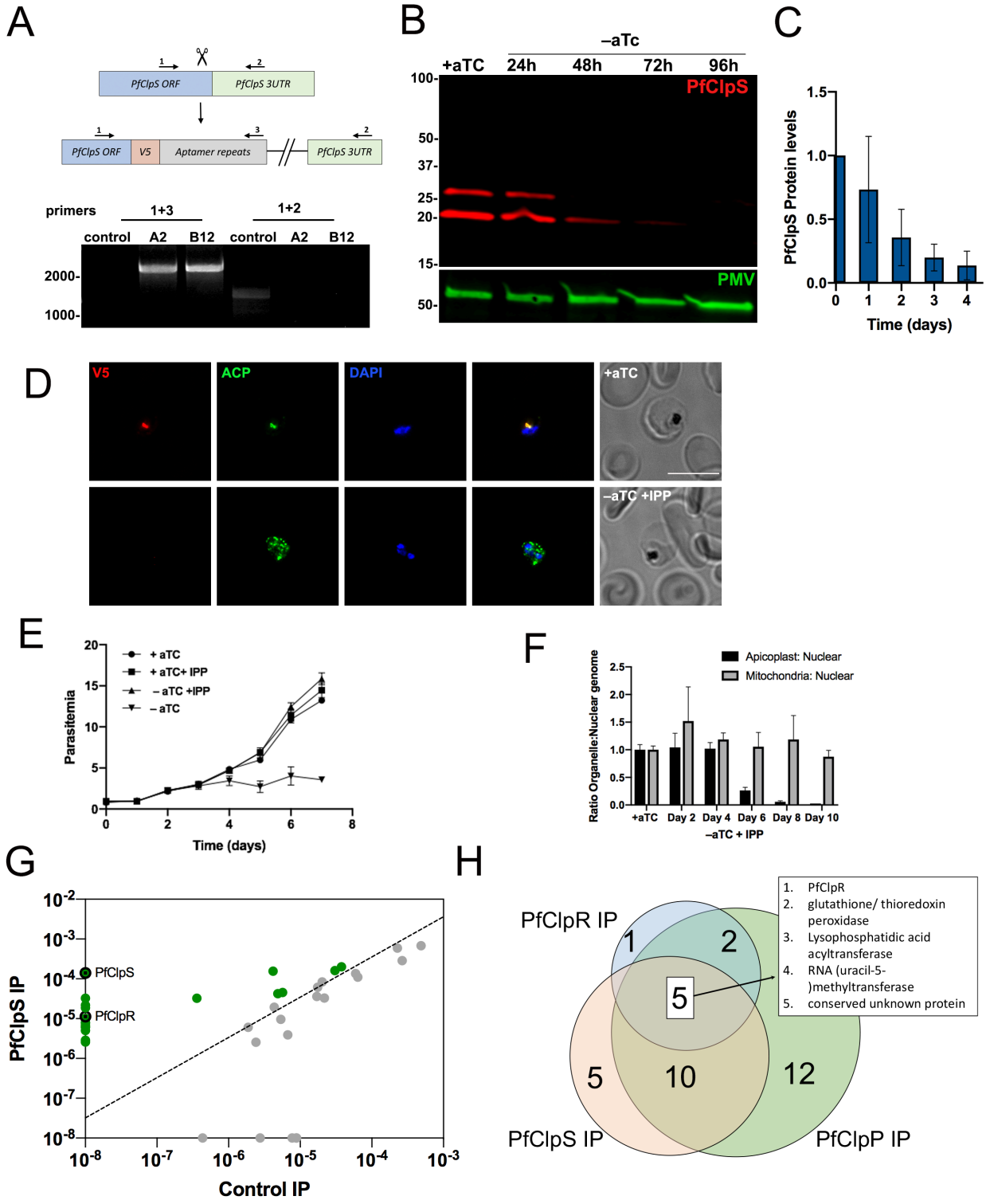
A
PfClpS ORF
PfClpS 3UTR
PfClpS ORF
V5
Aptamer repeats
PfClpS 3UTR
primers
1+3
1+2
control
A2
B12
control
A2
B12
2000-
1000-
B
–aTc
+aTC
24h
48h
72h
96h
PfClpS
PMV
100-
50-
37-
25-
20-
15-
50-
C
PfClpS Protein levels
Time (days)
D
V5
ACP
DAPI
+aTC
–aTC +IPP
E
+ aTC
+ aTC+ IPP
– aTC +IPP
– aTC
Parasitemia
Time (days)
F
Apicoplast: Nuclear
Mitochondria: Nuclear
Ratio Organelle:Nuclear genome
+aTC
Day 2
Day 4
Day 6
Day 8
Day 10
–aTC + IPP
G
PfClpS
PfClpR
PfClpS IP
Control IP
H
PfClpR IP
PfClpS IP
PfClpP IP
1
2
5
5
10
12
1. PfClpR
2. glutathione/ thioredoxin peroxidase
3. Lysophosphatidic acid acyltransferase
4. RNA (uracil-5-)methyltransferase
5. conserved unknown protein

703 **Figure 5**

704 A. Upper panel: Diagram showing integration of the *tetR*-aptamer cassette into the *pfclps* locus.
705 Cas9 nuclease with the gRNA introduces a double-stranded break at the beginning of the C-
706 terminus of the *pfclps* gene. The repair plasmid provides homology regions for double-
707 crossover homologous recombination, introducing a 3xV5 tag and the *tetR*-aptamer cassette.
708 Lower panel: PCR test confirming *tetR*-aptamer integration at the *pfclps* locus. gDNA was
709 purified from transfected parasites. Primers 1+2 or 1+3 (see methods) were used to amplify
710 the native locus or an integration specific band, as illustrated in the diagram.

711 B. PfClpS^{apt} parasites were incubated without aTc for 4 days, and lysates were isolated every 24
712 hr. Western blot of parasite lysates probed with antibodies against V5 (PfClpS, red) and
713 Plasmepsin V (PMV, loading control, green). A significant reduction in PfClpS protein levels in
714 apparent after 72 hours. The protein marker sizes that co-migrated with the probed protein
715 are shown on the left.

716 C. Quantification of PfClpS knockdown (as shown in B, n= 3 biological replicates). Values were
717 normalized to PfClpS levels in the presence of aTc.

718 D. Immunofluorescence microscopy of fixed PfClpS^{apt} parasites that were incubated for 8 days
719 with aTc (upper panel) or without aTc and supplemented with IPP (lower panel). Parasites
720 were stained with antibodies against V5 (PfClpS, red), ACP (Acyl Carrier Protein, green), and
721 DAPI (DNA). PfClpS localizes to the apicoplast when aTc is present. Upon aTc removal, PfClpS
722 disappears and ACP appears in vesicle-like structures. Z-stack images were deconvolved and
723 projected as a combined single image. Representative images from one of two biological
724 replicates are shown. Scale bar, 5μm.

725 E. PfClpS^{apt} parasites (Clone A2) were grown with or without aTc and IPP, and parasitemia was
726 monitored every 24 hr over 7 days via flow cytometry. Parasites grown without aTc exhibit a
727 growth defect by day 4, and they die in the following days. Addition of IPP rescues the growth
728 defect, indicating an apicoplast damage. 100% of growth represents the highest value of
729 calculated parasitemia (final parasitemia in the presence of aTc). Data are represented as
730 mean ± SEM (n= 3 technical replicates). One representative experiment out of three biological
731 replicates is shown.

732 F. Synchronized PfClpS^{apt} parasites were grown in the absence of aTc and presence of IPP.
733 Genomic DNA samples were taken at the beginning of each replication cycle for real-time
734 qPCR analysis. Apicoplast: nuclear genome ratio was calculated every 48h. Mitochondria:
735 nuclear genome ratio served as a control. Genome ratios were normalized to parasites grown
736 in the presence of aTc. Data are represented as mean ± SEM (n= 3 technical replicates). One
737 representative experiment out of three biological replicates is shown.
738 G. Mass spectrometry analysis of PfClpS immunoprecipitated from PfClpS^{apt} parasites using anti
739 V5 antibody-conjugated beads. The parental line 3D7 was used a control and pulldown
740 experiments were done in duplicates. 10^9 parasites pellets were isolated and incubated with
741 anti-V5 crosslinked-beads. Samples were analyzed by mass spectrometry. All detected
742 proteins detected in biological replicates were filtered for predicted apicoplast localization.
743 The abundance of each apicoplast-predicted protein was calculated and averaged between
744 replicates. To filter for high confidence hits, we set a threshold of ≥5 folds enrichment in
745 PfClpS vs. parental control. PfClpS IP yielded 30 apicoplast-localized proteins, out of which 20
746 have passed the threshold and were defined as high-confidence hits, including PfClpR.
747 H. Venn diagram showing the overlap between PfClpS, PfClpP and PfClpR high-confidence
748 interactors. Out of the 35-total high-confidence hits, 17 are shared between more than one
749 Clp IP and 5 proteins were identified in all 3 proteomic experiments

750 **Figure 6**

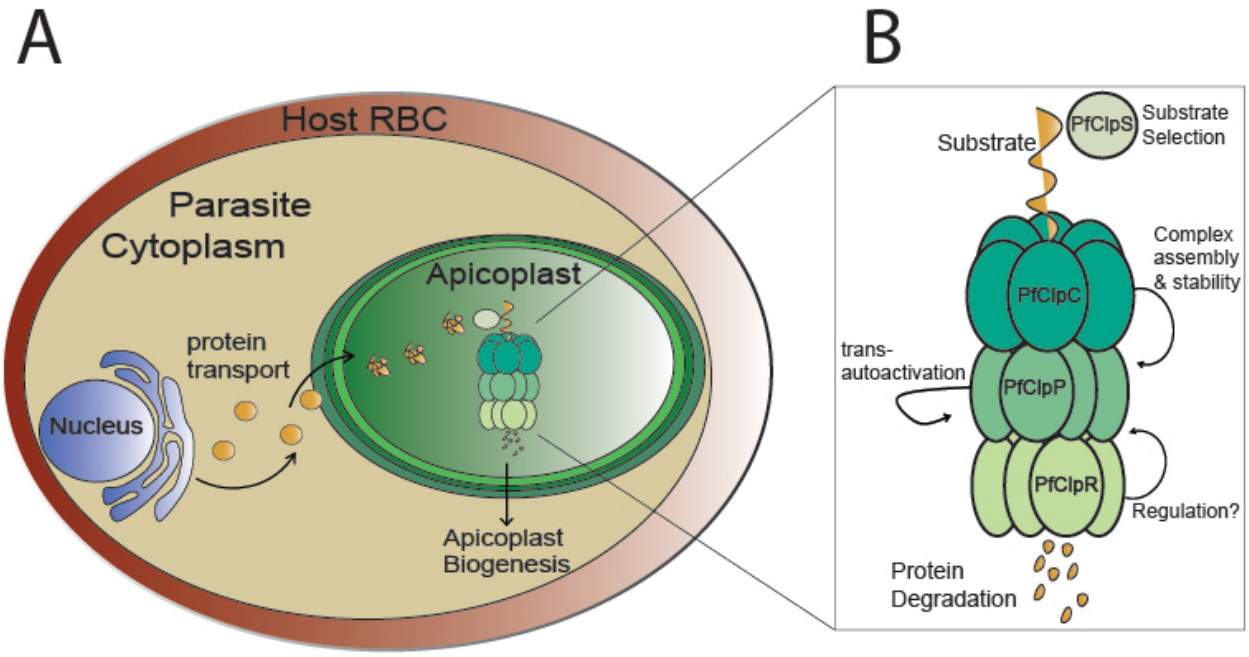

751 **Figure 6**

752 A. The Clp complex is a master regulator of apicoplast biology. Most of apicoplast proteins are
753 encoded by the cell nucleus, and are transported to the organelle via the secretory pathway.
754 According to this model, the apicoplast does not control their synthesis, and therefore a
755 stable proteome in the organelle is maintained via protein degradation. This central function
756 is required, among other things, for organelle biogenesis, and is executed and regulated by
757 the proteolytic Clp complex. As a consequence, interfering with the function of different
758 subunits of the complex leads to organelle loss and parasite death.

759 B. Molecular function of the apicoplast Clp system. In the core of the Clp complex is PfClpP, a
760 conserved potent serine protease. PfClpP oligomerizes as a zymogen and then matures
761 through trans-autoprocessing. PfClpR is a non-catalytic subunit that interacts with other Clp
762 proteins and may have a regulatory role. PfClpC is the chaperone that unfolds proteins and
763 feed them into the PfClpP proteolytic core. A transient interaction between PfClpC and the
764 mature PfClpP is crucial for complex stability and function. A small adaptor molecule, PfClpS,
765 binds and selects specific substrates for delivery to the complex.

766

767 **Supplementary Figure 1**

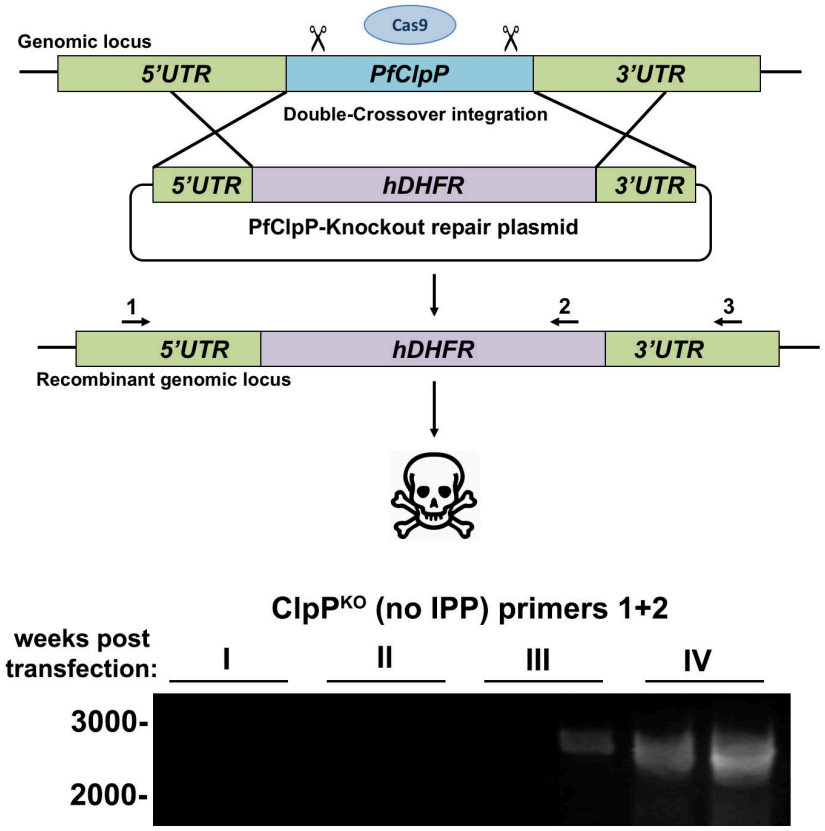

768

769 **Supplementary Figure 1**

770 A diagram depicting the generation of PfClpP knockout (PfClpP^{KO}) parasites. Cas9 nuclease
771 and two guide RNAs targeting the N- and the C-termini of PfClpP were used to facilitate
772 integration. The repair plasmid contained 500bps homology regions to the 5'UTR and the
773 3'UTR of the *pfclpp* locus flanking a drug marker (hDHFR, human Dihydrofolate Reductase).
774 Through double crossover integration and drug selection, the gene was replaced with the
775 drug marker. Despite evidence for integration into the genomic locus (bottom), this strategy
776 failed to retrieve live parasites in the absence of IPP, indicating the PfClpP is essential to
777 parasite viability due to its apicoplast function.

778 **Supplementary Figure 2**

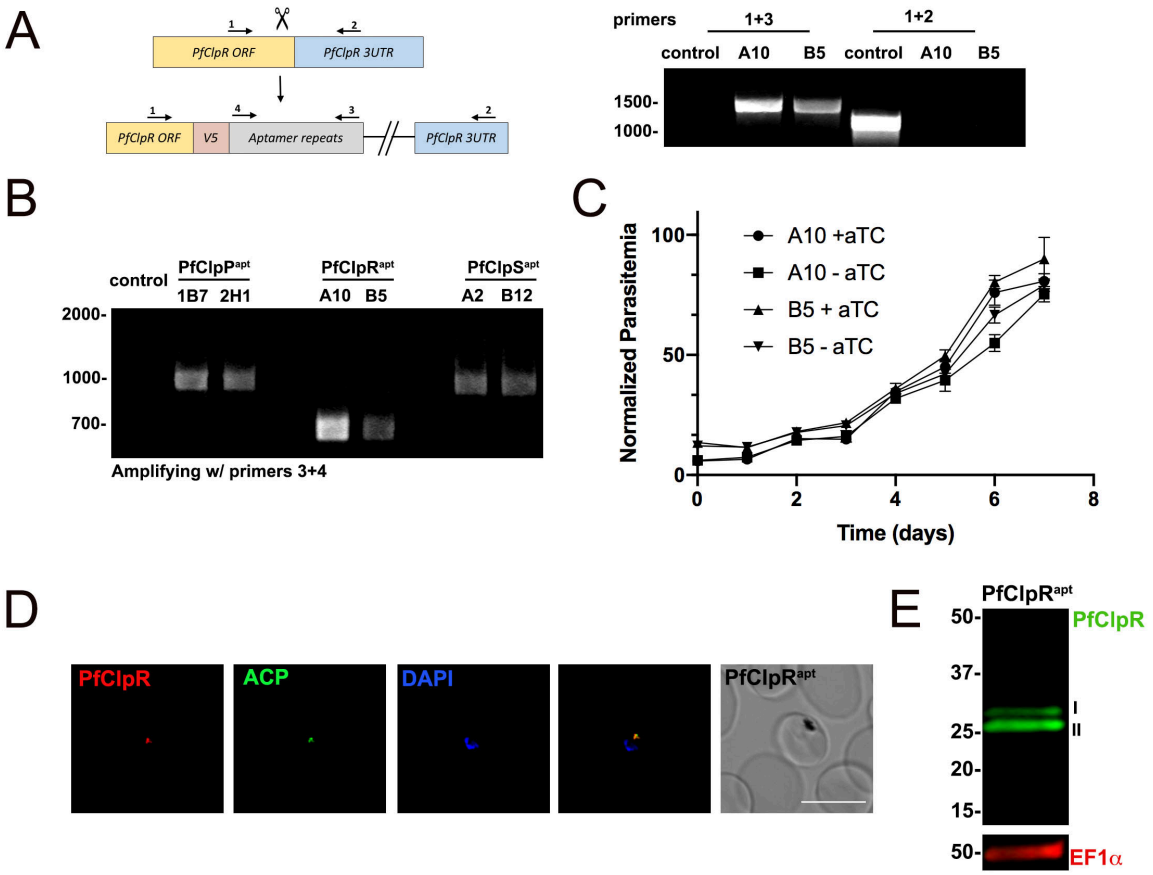

779 **Supplementary Figure 2**

780 A. Diagram showing integration of the *tetR*-aptamer system into the *pfclpr* locus. Cas9 nuclease
781 with a specific guide RNA introduces a double-stranded break at the C-terminus of the *pfclpr*
782 gene. The repair plasmid provides homology regions for double-crossover homologous
783 recombination, introducing a 3xV5 tag and the *tetR*-aptamer cassette.
784 PCR test confirming *tetR-aptamer* integration at the *pfclpr* locus. Genomic DNA was purified
785 from 2 mutant clones (A10 and B5). Primers 1,2,3 (see methods) were used to amplify the
786 native locus (1+2) or an integration specific product (1+3), as illustrated in the diagram.
787 B. PCR test to evaluate aptamer repeat numbers in *tetR*-aptamer cassette in genomic DNA
788 isolated from PfClpP^{apt}, PfClpR^{apt}, and PfClpS^{apt} clones. The original plasmid contained 10
789 aptamer repeats, each 100pb long. Reduction in repeats numbers implies decreased binding
790 by the *tet*-Repressor which compromises knockdown efficiency. While PfClpP^{apt} and PfClpS^{apt}

791 clones show the expected 1 kb PCR product which corresponds to 10 aptamer repeats, all
792 PfClpR^{apt} clones show a 0.7 kb product, indicating the loss of 3 aptamer repeats.

793 C. Two PfClpR^{apt} clones (A5 and B10) were grown with or without 0.5 uM aTc, and parasitemia
794 was monitored every 24 hr over 11 days via flow cytometry. 100% of growth represents the
795 highest value of calculated parasitemia (final parasitemia in the presence of aTc). Data are
796 represented as mean ± SEM (n= 3 technical replicates). One representative experiment out
797 of two biological replicates is shown.

798 D. Immunofluorescence microscopy of fixed PfClpR^{apt} parasites stained with antibodies against
799 V5 (PfClpR^{apt}, red), ACP (Acyl Carrier Protein, green), and DAPI (DAPI). Z-stack images were
800 deconvolved and projected as a combined single image. Representative images from one of
801 two biological replicates are shown. Scale bar, 5μm.

802 E. PfClpR^{apt} lysates were isolated and probed with antibodies against V5 (PfClpR^{apt}, red), and
803 PMV (loading control). The doublet observed for PfClpR is typical for apicoplast proteins and
804 include a cytoplasmic fraction (I) and an apicoplast-localized protein after the transit peptide
805 had been removed (II). The protein marker sizes that co-migrated with the probed protein
806 are shown on the left.

807 **Supplementary Figure 3**

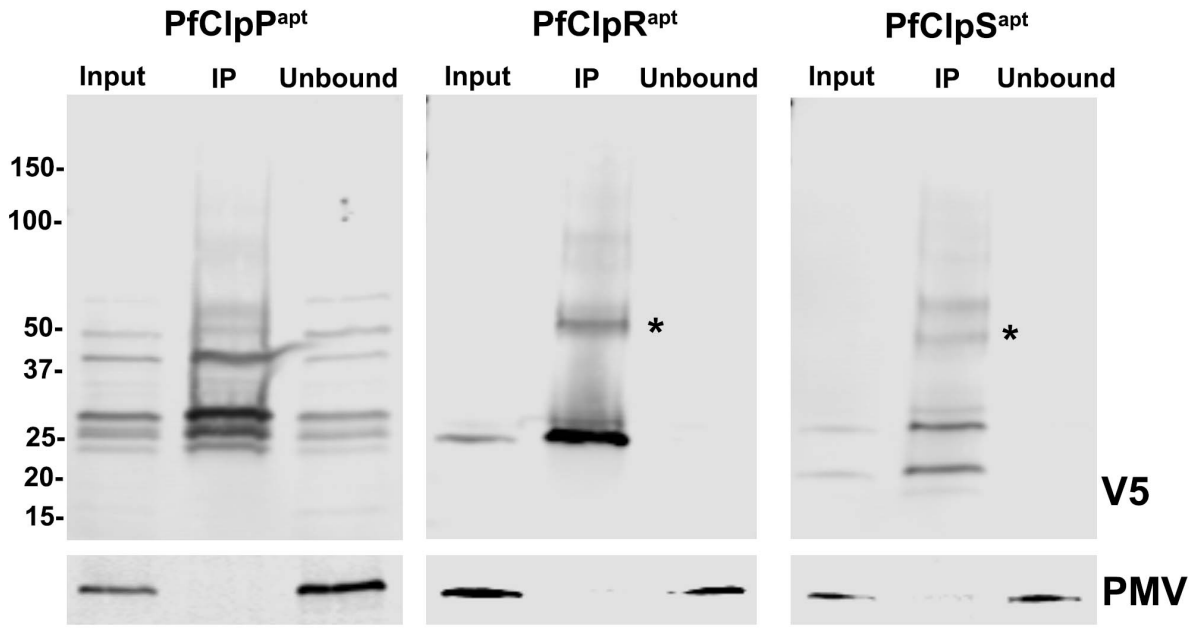

808 **Supplementary Figure 3**

809 Immunoprecipitation of PfClpP^{apt}, PfClpR^{apt} and PfClpS^{apt} for proteomic analysis. 10^9 parasites
810 were isolated and 10% of the volume was saved as an input sample. Immunoprecipitation of the
811 tagged proteins from respective parasite lysates were performed using anti-V5 antibody-
812 conjugated beads. Input, IP and unbound samples were separated on SDS-PAGE and blotted with
813 anti-V5 antibodies and anti-PMV (Plasmpesin V, loading control). The heavy chain of the antibody
814 that eluted with some of the IP samples, despite cross linking is shown (*).

815

816 ## References

817 1. McFadden, G. I., Reith, M. E., Munholland, J. & Lang-Unnasch N. Plastid in human
818 parasites. *Nature* **381,** 482–482 (1996).
819 2. Köhler, S., Delwiche, C. F., Denny, P. W., Tilney, L. G., Webster, P., Wilson, R. J., Palmer, J.
820 D. & Roos, D. S. A plastid of probable green algal origin in Apicomplexan parasites.
821 *Science* **275,** 1485–1489 (1997).
822 3. van Dooren, G. G. & Striepen, B. The algal past and parasite present of the apicoplast.
823 *Annu. Rev. Microbiol.* **67,** 271–289 (2013).
824 4. Ralph, S. A., Foth, B. J., Hall, N. & McFadden, G. I. Evolutionary Pressures on Apicoplast
825 Transit Peptides. *Mol Biol Evol* **21,** 2183–2194 (2004).
826 5. Fichera, M. E. & Roos, D. S. A plastid organelle as a drug target in apicomplexan parasites.
827 *Nature* **390,** 407–409 (1997).
828 6. Dahl, E. L., & Rosenthal, P. J. Multiple Antibiotics Exert Delayed Effects against the
829 Plasmodium falciparum Apicoplast. *Antimicrobial Agents and Chemotherapy* **51,** 3485–
830 3490 (2007).
831 7. Borrmann, S., Issifou, S., Esser, G., Adegnika, A. A., Ramharter, M., Matsiegui, P.-B.,
832 Oyakhirome, S., Mawili-Mboumba, D. P., Missinou, M. A., Kun, J. F. J., Jomaa, H. &
833 Kremsner, P. G. Fosmidomycin-clindamycin for the treatment of Plasmodium falciparum
834 malaria. *J Infect Dis.* **190,** 1534–1540 (2004).
835 8. Sponer, U., Prajakwong, S., Wiedermann, G., Kollaritsch, H., Wernsdorfer, G. &
836 Wernsdorfer, W. H. Pharmacodynamic interaction of doxycycline and artemisinin in
837 Plasmodium falciparum. *Antimicrobial Agents and Chemotherapy* **46,** 262–264 (2002).
838 9. Dahl, E. L., Shock, J. L., Shenai, B. R., Gut, J., DeRisi, J. L. & Rosenthal, P. J. Tetracyclines
839 specifically target the apicoplast of the malaria parasite Plasmodium falciparum.
840 *Antimicrobial Agents and Chemotherapy* **50,** 3124–3131 (2006).
841 10. Goodman, C. D., Su, V. & McFadden, G. I. The effects of anti-bacterials on the malaria
842 parasite Plasmodium falciparum. *Molecular and Biochemical Parasitology* **152,** 181–191
843 (2007).

844 11. Waller, R. F., Reed, M. B., Cowman, A. F. & McFadden, G. I. Protein trafficking to the
845 plastid of Plasmodium falciparum is via the secretory pathway. *EMBO J* **19,** 1794–1802
846 (2000).
847 12. van Dooren, G. G., Su, V., D'Ombrain, M. C. & McFadden, G. I. Processing of an Apicoplast
848 Leader Sequence inPlasmodium falciparum and the Identification of a Putative Leader
849 Cleavage Enzyme. *Journal of Biological Chemistry* **277,** 23612–23619 (2002).
850 13. Foth, B. J., Ralph, S. A., Tonkin, C. J., Struck, N. S., Fraunholz, M., Roos, D. S., Cowman, A.
851 F. & McFadden, G. I. Dissecting Apicoplast Targeting in the Malaria Parasite Plasmodium
852 falciparum. *Science* **299,** 705–708 (2003).
853 14. Yeh, E. & DeRisi, J. L. Chemical rescue of malaria parasites lacking an apicoplast defines
854 organelle function in blood-stage Plasmodium falciparum. *PLoS Biol* **9,** e1001138 (2011).
855 15. Florentin, A., Cobb, D. W., Fishburn, J. D., Cipriano, M. J., Kim, P. S., Fierro, M. A.,
856 Striepen, B. & Muralidharan, V. PfClpC Is an Essential Clp Chaperone Required for Plastid
857 Integrity and Clp Protease Stability in Plasmodium falciparum. *Cell Rep* **21,** 1746–1756
858 (2017).
859 16. Olivares, A. O., Baker, T. A. & Sauer, R. T. Mechanistic insights into bacterial AAA+
860 proteases and protein-remodelling machines. *Nat Rev Micro* **14,** 33–44 (2016).
861 17. Nishimura, K. & van Wijk, K. J. Organization, function and substrates of the essential Clp
862 protease system in plastids. *Biochimica et Biophysica Acta* **1847,** 915–930 (2015).
863 18. Weber-Ban, E. U., Reid, B. G., Miranker, A. D. & Horwich, A. L. Global unfolding of a
864 substrate protein by the Hsp100 chaperone ClpA. *Nature* **401,** 90–93 (1999).
865 19. Kim, Y.-I., Levchenko, I., Fraczkowska, K., Woodruff, R. V., Sauer, R. T. & Baker, T. A.
866 Molecular determinants of complex formation between Clp/Hsp100 ATPases and the
867 ClpP peptidase. *Nature Structural & Molecular Biology* **8,** 230–233 (2001).
868 20. Frees, D., Gerth, U. & Ingmer, H. Clp chaperones and proteases are central in stress
869 survival, virulence and antibiotic resistance of Staphylococcus aureus. *International*
870 *Journal of Medical Microbiology* **304,** 142–149 (2014).
871 21. Rodríguez-Concepción, M., D'Andrea, L. & Pulido, P. Control of plastidial metabolism by
872 the Clp protease complex. *J. Exp. Bot.* **70,** 2049–2058 (2018).

873 22. Bakkouri, El, M., Pow, A., Mulichak, A., Cheung, K. L. Y., Artz, J. D., Amani, M., Fell, S., de
874 Koning-Ward, T. F., Goodman, C. D., McFadden, G. I., Ortega, J., Hui, R. & Houry, W. A.
875 The Clp chaperones and proteases of the human malaria parasite Plasmodium
876 falciparum. *Journal of Molecular Biology* **404,** 456–477 (2010).
877 23. Bakkouri, El, M., Rathore, S., Calmettes, C., Wernimont, A. K., Liu, K., Sinha, D., Asad, M.,
878 Jung, P., Hui, R., Mohmmed, A. & Houry, W. A. Structural insights into the inactive
879 subunit of the apicoplast-localized caseinolytic protease complex of Plasmodium
880 falciparum. *Journal of Biological Chemistry* **288,** 1022–1031 (2013).
881 24. AhYoung, A. P., Koehl, A., Vizcarra, C. L., Cascio, D. & Egea, P. F. Structure of a putative
882 ClpS N-end rule adaptor protein from the malaria pathogen Plasmodium falciparum.
883 *Protein Science* **25,** 689–701 (2016).
884 25. Ganesan, S. M., Falla, A., Goldfless, S. J., Nasamu, A. S. & Niles, J. C. Synthetic RNA-
885 protein modules integrated with native translation mechanisms to control gene
886 expression in malaria parasites. *Nature Communications* **7,** 10727 (2016).
887 26. Wilson, R. H. & Hayer-Hartl, M. Complex Chaperone Dependence of Rubisco Biogenesis.
888 *Biochemistry* **57,** 3210–3216 (2018).
889 27. Muralidharan, V., Oksman, A., Pal, P., Lindquist, S. & Goldberg, D. E. Plasmodium
890 falciparum heat shock protein 110 stabilizes the asparagine repeat-rich parasite
891 proteome during malarial fevers. *Nature Communications* **3,** 1310 (2012).
892 28. Montandon, C., Friso, G., Liao, J.-Y. R., Choi, J. & van Wijk, K. J. In Vivo Trapping of
893 Proteins Interacting with the Chloroplast CLPC1 Chaperone: Potential Substrates and
894 Adaptors. *J. Proteome Res.* **18,** 2585–2600 (2019).
895 29. Flynn, J. M., Neher, S. B., Kim, Y.-I., Sauer, R. T. & Baker, T. A. Proteomic discovery of
896 cellular substrates of the ClpXP protease reveals five classes of ClpX-recognition signals.
897 *Mol. Cell* **11,** 671–683 (2003).
898 30. Trentini, D. B., Suskiewicz, M. J., Heuck, A., Kurzbauer, R., Deszcz, L., Mechtler, K. &
899 Clausen, T. Arginine phosphorylation marks proteins for degradation by a Clp protease.
900 *Nature* **539,** 48–53 (2016).

901 31. Erbse, A., Schmidt, R., Bornemann, T., Schneider-Mergener, J., Mogk, A., Zahn, R.,
902 Dougan, D. A. & Bukau, B. ClpS is an essential component of the N-end rule pathway in
903 Escherichia coli. *Nature* **439,** 753–756 (2006).
904 32. Hou, J. Y., Sauer, R. T. & Baker, T. A. Distinct structural elements of the adaptor ClpS are
905 required for regulating degradation by ClpAP. *Nature Structural & Molecular Biology* **15,**
906 288–294 (2008).
907 33. Nishimura, K., Asakura, Y., Friso, G., Kim, J., Oh, S.-H., Rutschow, H., Ponnala, L. & van
908 Wijk, K. J. ClpS1 is a conserved substrate selector for the chloroplast Clp protease system
909 in Arabidopsis. *The Plant Cell* **25,** 2276–2301 (2013).
910 34. Martin, A., Baker, T. A. & Sauer, R. T. Distinct static and dynamic interactions control
911 ATPase-peptidase communication in a AAA+ protease. *Mol. Cell* **27,** 41–52 (2007).
912 35. Gersch, M., Famulla, K., Dahmen, M., Göbl, C., Malik, I., Richter, K., Korotkov, V. S., Sass,
913 P., Rübsamen-Schaeff, H., Madl, T., Brötz-Oesterhelt, H. & Sieber, S. A. AAA+ chaperones
914 and acyldepsipeptides activate the ClpP protease via conformational control. *Nature*
915 *Communications* **6,** 6320 (2015).
916 36. Hackl, M. W., Lakemeyer, M., Dahmen, M., Glaser, M., Pahl, A., Lorenz-Baath, K., Menzel,
917 T., Sievers, S., Böttcher, T., Antes, I., Waldmann, H. & Sieber, S. A. Phenyl Esters Are
918 Potent Inhibitors of Caseinolytic Protease P and Reveal a Stereogenic Switch for
919 Deoligomerization. *J. Am. Chem. Soc.* **137,** 8475–8483 (2015).
920 37. Brötz-Oesterhelt, H. & Sass, P. Bacterial caseinolytic proteases as novel targets for
921 antibacterial treatment. *International Journal of Medical Microbiology* **304,** 23–30
922 (2014).
923 38. Böttcher, T. & Sieber, S. A. β-Lactones as Specific Inhibitors of ClpP Attenuate the
924 Production of Extracellular Virulence Factors of Staphylococcus aureus. *J. Am. Chem. Soc.*
925 **130,** 14400–14401 (2008).
926 39. Conlon, B. P., Nakayasu, E. S., Fleck, L. E., LaFleur, M. D., Isabella, V. M., Coleman, K.,
927 Leonard, S. N., Smith, R. D., Adkins, J. N. & Lewis, K. Activated ClpP kills persisters and
928 eradicates a chronic biofilm infection. *Nature* **503,** 365–370 (2013).

929 40. Ghorbal, M., Gorman, M., Macpherson, C. R., Martins, R. M., Scherf, A. & Lopez-Rubio, J.-
930 J. Genome editing in the human malaria parasite Plasmodium falciparum using the
931 CRISPR-Cas9 system. *Nature Biotechnology* **32,** 819–821 (2014).
932 41. Cobb, D. W., Florentin, A., Fierro, M. A., Krakowiak, M., Moore, J. M. & Muralidharan, V.
933 The Exported Chaperone PfHsp70x Is Dispensable for the Plasmodium falciparum
934 Intraerythrocytic Life Cycle. *mSphere* **2,** e00363–17 (2017).
935 42. Kudyba, H. M., Cobb, D. W., Florentin, A., Krakowiak, M. & Muralidharan, V. CRISPR/Cas9
936 Gene Editing to Make Conditional Mutants of Human Malaria Parasite P. falciparum. *J Vis*
937 *Exp* (2018). doi:10.3791/57747
938 43. Muralidharan, V., Oksman, A., Iwamoto, M., Wandless, T. J. & Goldberg, D. E. Asparagine
939 repeat function in a Plasmodium falciparum protein assessed via a regulatable
940 fluorescent affinity tag. *Proceedings of the National Academy of Sciences* **108,** 4411–4416
941 (2011).
942 44. Kudyba, H. M., Cobb, D. W., Fierro, M. A., Florentin, A., Ljolje, D., Singh, B., Lucchi, N. W.
943 & Muralidharan, V. The endoplasmic reticulum chaperone PfGRP170 is essential for
944 asexual development and is linked to stress response in malaria parasites. *Cellular*
945 *Microbiology* **23,** e13042 (2019).
946 45. Zuegge, J., Ralph, S., Schmuker, M., McFadden, G. I. & Schneider, G. Deciphering
947 apicoplast targeting signals--feature extraction from nuclear-encoded precursors of
948 Plasmodium falciparum apicoplast proteins. *Gene* **280,** 19–26 (2001).
949 46. Cilingir, G., Broschat, S. L. & Lau, A. O. T. ApicoAP: the first computational model for
950 identifying apicoplast-targeted proteins in multiple species of Apicomplexa. *PLoS ONE* **7,**
951 e36598 (2012).
952 47. Boucher, M. J., Ghosh, S., Zhang, L., Lal, A., Jang, S. W., Ju, A., Zhang, S., Wang, X., Ralph,
953 S. A., Zou, J., Elias, J. E. & Yeh, E. Integrative proteomics and bioinformatic prediction
954 enable a high-confidence apicoplast proteome in malaria parasites. *PLoS Biol* **16,**
955 e2005895 (2018).